Published in final edited form as:
Nat Immunol. 2020 January ; 21(1): 75–85. doi:10.1038/s41590-019-0555-2.

An intrinsic role of IL-33 in T_{reg} cell-mediated tumor immunoevasion

Aikaterini Hatzioannou[1], **Aggelos Banos**[1], **Theodore Sakelaropoulos**[2,3], **Constantinos Fedonidis**[4], **Maria-Sophia Vidali**[5], **Maren Köhne**[6], **Kristian Händler**[7], **Louis Boon**[8], **Ana Henriques**[9], **Vasiliki Koliaraki**[9], **Panagiotis Georgiadis**[5], **Jerome Zoidakis**[10], **Aikaterini Termentzi**[11], **Marc Beyer**[6,7], **Triantafyllos Chavakis**[12,13], **Dimitrios Boumpas**[1,14], **Aristotelis Tsirigos**[2], **Panayotis Verginis**[1,12]

[1]Center of Clinical, Experimental Surgery & Translational Research, Biomedical Research Foundation Academy of Athens, Greece [2]Applied Bioinformatics Laboratories, New York University School of Medicine, New York, NY, USA and Department of Pathology, New York University School of Medicine, New York, NY, USA [3]Laura and Isaac Perlmutter Cancer Center, NYU School of Medicine, New York, NY 10016, USA [4]Center of Basic Research, Biomedical Research Foundation Academy of Athens, Greece [5]Institute of Biology, Medicinal Chemistry & Biotechnology, National Hellenic Research Foundation, Greece [6]Molecular Immunology in Neurodegeneration, German Center for Neurodegenerative Diseases (DZNE), Sigmund-Freud-Str. 27, 53127 Bonn, Germany [7]PRECISE, Platform for Single Cell Genomics and Epigenomics at the German Center for Neurodegenerative Diseases and the University of Bonn, Sigmund-Freud-Str. 27, 53127 Bonn, Germany [8]Bioceros BV, Utrecht, Netherlands [9]Department of Immunology, Biomedical Sciences Research Centre "Alexander Fleming," Vari, Greece [10]Biotechnology Division, Biomedical Research Foundation of the Academy of Athens, Athens, Greece [11]Department of Pesticides Control and Phytopharmacy, Benaki Phytopathological Institute, Athens, Greece [12]Institute for Clinical Chemistry and Laboratory Medicine, University Hospital and Faculty of Medicine Carl Gustav Carus of TU Dresden, Dresden, Germany [13]National Center for Tumor Diseases (NCT), Partner Site Dresden, and German Cancer Research Center, Heidelberg, Germany [14]Joint Rheumatology Program, 4th Department of Internal Medicine, Attikon University Hospital, National and Kapodistrian University of Athens Medical School, Athens, Greece

Corresponding author: Panayotis Verginis, Clinical, Experimental Surgery & Translational Research, Biomedical Research Foundation Academy of Athens, 4 Soranou Ephessiou Str, 11527 Athens, Greece, Phone/Fax: 00302106597516, pverginis@bioacademy.gr.

Data availability

The data that support the findings of this study are available from the corresponding author upon reasonable request.

Author Contributions

A.Ha., A.B. designed and performed experiments, analyzed data, generated figures, and wrote the manuscript. C.F., M.-S.V., M.K., K.H., A.He. performed experiments and analyzed data. L.B. generated and provided critical reagents. T.S. and A.Ts assisted with mRNAseq and ATAC-seq data analysis, interpretation and T.S. generated figures. J.Z. and A.Te. performed and analyzed the targeted proteomics experiments. V.K., P.G. and M.B. contributed in data analysis and interpretation. T.C. and D.B. interpreted data. P.V. designed and supervised the study, performed data analysis, and wrote the manuscript.

Competing Interests

The authors declare no competing interests.

Europe PMC Funders Author Manuscripts

Europe PMC Funders Author Manuscripts

Abstract

Regulatory T (T_{reg}) cells accumulate into tumors hindering the success of cancer immunotherapy. Yet, therapeutic targeting of T_{reg} cells shows limited efficacy or leads to autoimmunity. The molecular mechanisms that guide T_{reg} cell stability in tumors, remain elusive. Herein, we identify a cell-intrinsic role of the alarmin IL-33 in the functional stability of T_{reg} cells. Specifically, IL-33-deficient T_{reg} cells demonstrated attenuated suppressive properties in vivo and facilitated tumor regression in an ST2 (IL-33 receptor)-independent fashion. Upon activation, *Il33*$^{-/-}$ T_{reg} cells exhibited epigenetic reprogramming with increased chromatin accessibility of the *Ifng* locus leading to elevated interferon-γ (IFN-γ) production in an NF-κB–T-bet-dependent manner. IFN-γ was essential for T_{reg} cell defective function since its ablation restored *Il33*$^{-/-}$ T_{reg} cell suppressive properties. Importantly, genetic ablation of *Il33* potentiated the therapeutic effect of immunotherapy. Our findings reveal a novel and therapeutically important intrinsic role of IL-33 in T_{reg} cell stability in cancer.

Introduction

Foxp3^{+} regulatory T (T_{reg}) cells play an instrumental role in immune homeostasis and maintenance of self-tolerance while their absence leads to fatal autoimmunity[1]. T_{reg} cells are enriched in the circulation and tumor microenvironment of cancer patients and their presence correlates with tumor progression, invasiveness and metastasis, where they hamper the success of cancer immunotherapy [2, 3]. T_{reg} cells represent a putative therapeutic target with checkpoint inhibitor-targeted immunotherapy against molecules mainly expressed by T_{reg} cells to demonstrate promising results. However, still cancer immunotherapy remains ineffective in a large proportion of patients, while responses are frequently accompanied by autoimmune manifestations [4, 5]. Consequently, an urgent need exists to precisely target the tumor-specific T_{reg} cells without affecting the peripheral T_{reg} cell repertoire. To achieve this goal, the molecular events that dictate the suppressive program of tumor T_{reg} cells need to be delineated.

Interleukin 33 (IL-33), an “alarmin” of the IL-1 family, has been correlated with the progression of several types of malignancies and is associated with low patient survival [6]. IL-33 is constitutively expressed by a broad range of stroma and hematopoietic cells acting as a transcription repressor released in the extracellular space upon cell death [6, 7]. Extracellular IL-33 binds to the suppression of tumorigenicity 2 receptor (ST2) and acts directly either on tumor cells enhancing their proliferation, invasion and migration or on endothelial cells promoting angiogenesis [8]. Although the impact of IL-33 in immune cell function during tumor immunosurveillance, remains unclear [8], in autoimmunity, IL-33–ST2 axis promotes T_{reg} cell stability, expansion and conversion of CD4^{+}Foxp3^{-}T cells to Foxp3-expressing inducible T_{reg} (iT_{reg}) cells [4, 8]. Whether extracellular IL-33 supports T_{reg} cell-mediated tumor-immune evasion and intranuclear IL-33 could shape the transcriptional landscape of T_{reg} cells and dictate their function in an anti-tumor immune response remain unexplored.

In this report, we describe a cell-intrinsic role of IL-33 in T_{reg} cell functional stability during tumor development. Ablation of IL-33 expression by Foxp3^{+} T_{reg} cells resulted in tumor

regression while IL-33-deficient T_{reg} cells exhibited impaired suppressive properties, promoted tumor eradication and evolution of robust anti-tumor immunity. Notably, in the absence of IL-33 T_{reg} cells maintained Foxp3 expression, consistent with a "fragile" phenotype [9, 10]. Epigenetic re-programming of tumor-exposed IL-33-deficient T_{reg} cells resulted in the up-regulation of IFN-γ expression, which accounted for T_{reg} cell dysfunction. Finally, genetic ablation of *Il33* potentiated the therapeutic efficacy of immunotherapy. Overall the findings presented here delineate a molecular program orchestrating T_{reg} cell stability within the tumor microenvironment.

Results

Tumor regression in IL-33-deficient mice

The precise role of IL-33 in anti-tumor immunity remains ill defined. To address IL-33 in tumors, we first performed a meta-analysis of The Cancer Genome Atlas (TCGA) Skin Cutaneous Melanoma (SCKM) dataset, which revealed a significant up-regulation of *Il33* expression and correlation with metastasis (Fig. 1a). In addition, IL-33 was increased in tumors (Fig. 1b) and tumor-draining lymph nodes (tdLNs) of B16.F10 melanoma cell (B16.F10)-inoculated compared to naïve animals and correlated to tumor progression (Fig. 1c), suggesting a role for IL-33 in promoting tumor growth. In support, B16.F10-inoculated IL-33-deficient mice (*Il33*$^{-/-}$) exhibited significantly reduced tumor growth compared to wild-type mice (Fig. 1d) accompanied by increased numbers of tumor-infiltrating $CD45^+$ leukocytes, $CD4^+$ and $CD8^+$ T cells (Fig. 1e,f). Paradoxically, frequencies and numbers of intratumoral $CD4^+Foxp3^+$ T_{reg} cells (Fig. 1e,f) were significantly elevated in *Il33*$^{-/-}$ animals. In a similar fashion, inoculation of *Il33*$^{-/-}$ mice with the poorly immunogenic Lewis lung carcinoma (LLC) cells, led to substantially diminished tumor growth but increased numbers of tumor-infiltrating $CD4^+Foxp3^+$ T_{reg} cells (Fig. 1g,h). To exclude immune cell alterations in *Il33*$^{-/-}$ mice at steady state, naive *Il33*$^{-/-}$ mice were compared to wild type animals. No differences were found in frequencies of $CD4^+$ T cells and $CD4^+Foxp3^+$ T_{reg} cells and expression of T_{reg} cell signature molecules, CD25 and glucocorticoid-induced TNFR-related protein (GITR), as well as the activation marker CD44 in the thymus and skin LNs (Supplementary Fig. 1a, b). Moreover, frequencies of $CD11c^+$ dendritic cells (DCs) and $CD11b^+$ monocytes in the bone marrow and spleen of the two groups did not demonstrate differences (Supplementary Fig. 1c). Overall, these findings suggested that IL-33 deficiency impaired tumor development and promoted the anti-tumor immunity with an unexpected increase in intratumoral $Foxp3^+$ T_{reg} cells.

Host-derived IL-33 directs tumor regression

IL-33 promotes T_{reg} cell proliferation [8] while tumor cells have been reported to produce substantial quantities of IL-33 [11]. Thus, we postulated that increase of tumor-infiltrating $Foxp3^+$ T_{reg} cells in *Il33*$^{-/-}$ mice might be due to tumor-derived IL-33. To address this, we engineered B16.F10 cells that lacked expression of endogenous IL-33 through shRNAs targeting of *Il33* gene. Thus, shIL-33_1 diminished IL-33 in both mRNA and protein levels compared to shIL-33_2 and scramble (Supplementary Fig. 2a), while B16.F10 transduction did not affect their viability and in vitro proliferation (Supplementary Fig. 2b). Therefore, B16.F10 cells transduced with shIL-33_1 (denoted as B16.F10$^{\Delta Il33}$) were used throughout

this study. Accordingly, B16.F10$^{\Delta Il33}$-inoculated *Il33*$^{-/-}$ mice presented significantly reduced tumor volume and tumor weight as well as delayed tumor growth compared to wild type animals (Fig. 2a). This finding was also evident by the significantly decreased proliferation of tumor cells based on Ki67 expression and decreased formation of tumor vessels as determined by CD31 and vascular cell adhesion protein 1 (VCAM) immunofluorescence staining (Fig. 2b). Tumor regression in B16.F10$^{\Delta Il33}$-inoculated *Il33*$^{-/-}$ mice was accompanied by increased numbers of tumor-infiltrating CD45^{+} leukocytes that exhibited elevated IFN-γ expression and increased numbers of CD4^{+} T cells (Fig. 2c,d), while NK1.1^{+} cell numbers were significantly reduced (Fig. 2c, Supplementary Fig. 2c). Furthermore, tumors from *Il33*$^{-/-}$ mice were enriched in activated myeloid cells as determined by MHC class II expression on CD11c^{+} DCs and CD11b^{+} monocytes (Fig. 2c,e, Supplementary Fig. 2c). Strikingly, the robust anti-tumor immunity in B16.F10$^{\Delta Il33}$-inoculated *Il33*$^{-/-}$ mice was associated with significantly elevated numbers of intratumoral Foxp3^{+} T$_{reg}$ cells (Fig. 2c). Of note, no significant differences in Ki67 expression (proliferation) or phospho-γH2AX expression indicative of DNA damage were observed by intratumoral Foxp3^{+} T$_{reg}$ cells in melanoma-bearing wild type and *Il33*$^{-/-}$ animals (Supplementary Fig. 2d). Together, these findings underscore that host-derived IL-33 deficiency was responsible for tumor regression.

Impaired suppressive function of *Il33*$^{-/-}$ T$_{reg}$ cells

Considering the pivotal role of Foxp3^{+} T$_{reg}$ cells in tumor development[2], we sought to investigate the contribution of the increased Foxp3^{+} T$_{reg}$ cell numbers in the anti-tumor immune response of B16.F10$^{\Delta Il33}$-inoculated *Il33*$^{-/-}$ mice. To address this, B16.F10$^{\Delta Il33}$-inoculated *Il33*$^{-/-}$ and wild type mice were treated with anti-CD25 monoclonal antibody that specifically depletes T$_{reg}$ cells [12]. Although depletion efficiency was similar in the two groups (Supplementary Fig. 3a), anti-CD25-treated wild type animals presented reduced tumor volume compared to non-treated control mice, while anti-CD25 treatment did not affect tumor growth in *Il33*$^{-/-}$ animals (Fig. 3a). These results suggested that depletion of T$_{reg}$ cells in IL-33 deficient mice did not further enhance tumor regression as was shown in wild type animals. Since IL-33 signals through its receptor ST2 on T$_{reg}$ cells to promote their stability and function[8], we asked whether IL-33-ST2 axis on T$_{reg}$ cells is implicated in tumor regression. To this end, we generated mice with ablation of MyD88, a major component of ST2-mediated signaling, in Foxp3^{+} T$_{reg}$ cells by crossing of *Myd88*$^{fl/fl}$ mice with *Foxp3*^{Cre} mice. No significant changes in tumor growth and frequencies of intratumoral CD45^{+}, CD4^{+} and CD4^{+}Foxp3^{+} T$_{reg}$ cells were monitored in B16.F10-inoculated *Foxp3*^{Cre}*Myd88*$^{fl/fl}$ mice compared to *Myd88*$^{fl/fl}$ control animals (Supplementary Fig. 3b). Since IL-33 signaling could occur independently of MyD88[13] we sorted highly pure CD4^{+}CD25^{hi}GITR^{+} T$_{reg}$ cells (>90% Foxp3^{+}) (Supplementary Fig. 3c) from either *St2*$^{+/+}$ or *St2*$^{-/-}$ mice and adoptively transferred them into *Rag1*$^{-/-}$ recipients (that lack T and B lymphocytes) that were reconstituted with *St2*$^{+/+}$CD4^{+}CD25^{-}Foxp3^{-} and CD8^{+} T effector cells and further inoculated with B16.F10$^{\Delta Il33}$ melanoma cells. Notably, no significant differences in tumor volume and tumor weight were observed in *Rag1*$^{-/-}$ mice that received *St2*$^{-/-}$ T$_{reg}$ cells compared to *St2*$^{+/+}$ T$_{reg}$ cells-transferred mice (Fig. 3b). Thus, ablation of ST2-mediated IL-33 signaling specifically in T$_{reg}$ cells did not alter their tumor-promoting function. These results raised the possibility of a cell intrinsic role of IL-33 in T$_{reg}$ cell

function. To address this, we first assessed *Il33* mRNA levels by *in vitro* activated CD4$^+$Foxp3$^+$ T_{reg} cells isolated from *Foxp3*^{gfp} reporter wild type or *Il33*$^{-/-}$ mice through qPCR. Indeed, *Il33* was expressed by activated T_{reg} cells from wild type mice but not from IL-33-deficient mice (Supplementary Fig. 3d). Importantly, a targeted proteomics approach for detecting IL-33 yielded a positive result in wild type T_{reg} cells for one out of the nine proteotypic peptides in the sequence of IL-33 (DYSVELQR, aminoacids 198-205) (Fig. 3c) that was undetected in *Il33*$^{-/-}$ T_{reg} cells (data not depicted). Based on our data showing that T_{reg} cells produce IL-33, we further explored its functional importance in tumor growth. Specifically, *Rag1*$^{-/-}$ mice adoptively transferred with *Il33*$^{-/-}$ Foxp3$^+$ T_{reg} cells from *Il33*$^{-/-}$ *Foxp3*^{gfp} mice in combination with *Il33*$^{+/+}$ CD4$^+$Foxp3$^-$ and CD8+ T cells exhibited markedly reduced tumor volume and tumor weight compared to *Il33*$^{+/+}$ T_{reg} cell-transferred mice (Fig. 3d) and accompanied by increased frequencies of intratumoral CD45$^+$ leukocytes and CD4$^+$ T cells (Fig. 3e). Importantly, we observed significant melanoma regression and delayed tumor growth in *Foxp*^{Cre}*Il33*$^{fl/fl}$ (specific ablation of IL-33 expression in T_{reg} cells) mice compared to control *Foxp3*^{Cre} mice (Fig. 3f), accompanied by increased numbers of tumor-infiltrating CD45$^+$ and Foxp3$^+$ T cells in comparison to control mice (Fig. 3g). Overall, these findings demonstrate an intrinsic role of IL-33 orchestrating the T_{reg} cell suppressive activity in tumor microenvironment.

IL-33-deficient Foxp3$^+$ T_{reg} cells present a "fragile" phenotype

To examine whether IL-33-deficient T_{reg} cells adopt an ex-T_{reg} cell phenotype, we assessed the methylation status of *Foxp3* T_{reg} cell-specific demethylated region (TSDR), which determines the stability of Foxp3 expression [14]. *Il33*$^{-/-}$ Foxp3^{gfp} T_{reg} cells displayed enhanced TSDR demethylation similar to *Il33*$^{+/+}$*Foxp3*^{gfp} T_{reg} cells (wild type T_{reg} cells), implying a stable Foxp3 expression (Fig. 4a). Interestingly, expression of cell surface molecules linked to Foxp3$^+$ T_{reg} suppressive activity, such as CTLA-4, LAG-3, GITR, killer cell lectin-like receptor subfamily G member 1 (KLRG-1), tumor necrosis factor receptor superfamily member 4 (OX-40) and inducible T-cell costimulator (ICOS) did not demonstrate any significant alteration in *Il33*$^{-/-}$*Foxp3*^{gfp} compared to *Il33*$^{+/+}$*Foxp3*^{gfp} T_{reg} cells from B16.F10$^{\Delta il33}$-inoculated animals. In contrast, we observed a significant up-regulation of PD-1 expression while expression of neuropilin (Nrp-1) was markedly reduced in *Il33*$^{-/-}$*Foxp3*^{gfp} T_{reg} cells (Fig. 4b) consistent with a "fragile" T_{reg} cell phenotype [9, 10]. Finally, assessment of the metabolic profile of tumor-infiltrating IL-33-deficient T_{reg} cells and in particular the mammalian target of rapamycin (mTORC-1) signaling that has been shown to impact on T_{reg} cell-mediated suppression [15], demonstrated increased abundance of phosphorylated mTOR, S6 and eukaryotic translation initiation factor 4E-binding protein 1 (4E-BP1) compared to wild type T_{reg} cells (Fig. 4c). Overall these data pointed towards a cell-intrinsic role of IL-33 in shaping the function and metabolic profile of Foxp3$^+$ T_{reg} cells in tumor microenvironment by hampering the induction of "fragile" Foxp3-expressing T_{reg} cells.

IFN-γ mediates the anti-tumor activity of *Il33*$^{-/-}$ T_{reg} cells

To investigate the transcriptional alterations that lead to the "fragile" phenotype of IL-33-deficient Foxp3$^+$ T_{reg} cells, highly pure CD4$^+$CD25$^+$GITR$^+$Foxp3$^+$ T_{reg} cells isolated from

tdLNs of B16.F10$^{\Delta Il33}$-inoculated *Il33*$^{-/-}$ and wild type animals were subjected to mRNA sequencing (RNAseq) revealing 585 differentially expressed genes in tumor-exposed *Il33*$^{-/-}$ T_{reg} cells compared to *Il33*$^{+/+}$ T_{reg} cells ($log_2FC > 0.4$ and adjusted p-value <0.05) (Fig. 5a). IL-33-sufficient and IL-33-deficient T_{reg} cells transcriptomes were clearly separated by distance clustering (Supplementary Fig. 4a). In accordance with the cell surface phenotype of *Il33*$^{-/-}$ Foxp3^{+} T_{reg} cells, no significant changes in T_{reg} cell-signature genes such as *Foxp3*, *Tgfb*, *Cd39*, *Ctla4*, *Granzyme*, *Perforin*, *Helios*, *Il7r*, *Gitr*, *Ox40*, *Ccdc22*, *Cmtm7* and *Ecm1* were observed (data not shown). Interestingly, *Ifng* listed among the upregulated genes of the prominent cluster of differentially expressed chemokines and cytokines (Fig. 5b). Increased expression and protein abundance of IFN-γ was validated in tumor-exposed *Il33*$^{-/-}$ Foxp3^{+} T_{reg} cells (Fig. 5c,d). Overall, gene expression data suggested a highly reshaped transcriptional landscape in IL-33-deficient T_{reg} cells correlating with a "T_{reg} cell-fragile" phenotype. Towards an in depth molecular mechanism delineation, transposase-accessible chromatin sequencing (ATAC-seq) revealed a significant altered chromatin landscape of *Il33*$^{-/-}$ T_{reg} cells compared to *Il33*$^{+/+}$ T_{reg} cells. Chromatin rearrangement was depicted in 1,432 differentially accessible regions (Figure 5e), distributed among promoters, introns and distal intergenic regions while the majority of these peaks concerned proximal promoters (-1 kb to transcription start site (TSS)) (Suppl. Fig 4b). Notably, data analysis with Genomic Regions Enrichment of Annotations Tool (GREAT) showed enrichment of genes implicated in IFN-γ pathway (Suppl. Fig 4c) while *Ifng* was among the genes that exhibit simultaneous differential chromatin accessibility and gene expression (Fig. 5f). Specifically, conserved non-coding region +17.703 to +20.863 kb to TSS (CNS +17/+19) of *Ifng* locus, which acts as a transcription enhancer [16], gained chromatin accessibility in tumor-exposed *Il33*$^{-/-}$compared to wild type T_{reg} cells (Fig 5g).

To investigate the functional importance of IFN-γ expression by *Il33*$^{-/-}$ T_{reg} cells, we crossed *Ifng*$^{-/-}$ animals with *Il33*$^{-/-}$*Foxp3*^{gfp} mice to generate IFN-γIL-33 double knockout mice (*Il33*$^{-/-}$*Ifng*$^{-/-}$). Adoptive transfer of highly pure *Il33*$^{-/-}$ *Ifng*$^{-/-}$*Foxp3*^{gfp} T_{reg} cells into T cell-reconstituted B16.F10$^{\Delta Il33}$-inoculated *Rag1*$^{-/-}$recipients demonstrated that ablation of IFN-γ restored the suppressive capacity of *Il33*$^{-/-}$Foxp3^{+} T cells and promoted tumor growth in contrast to *Il33*$^{-/-}$*Ifng*$^{+/+}$*Foxp3*^{gfp} T_{reg} cells (Fig. 5h). Collectively these findings revealed an essential role of IFN-γ in the functional re-programming of tumor-exposed *Il33*$^{-/-}$ Foxp3^{+} T_{reg} cells.

IFN-γ production by *Il33*$^{-/-}$ T_{reg} cells is dependent on NF-κB–T-bet axis

Next we sought to unravel the molecular events that drive IFN-γ up-regulation in IL-33-deficient Foxp3^{+} T_{reg} cells. Enrichment of differentially expressed transcriptional regulators that govern *Ifng* expression emerged from gene expression analysis of tumor-exposed *Il33*$^{-/-}$ T_{reg} cells (Fig. 6a) containing *Tbx21*, which encodes the transcription factor T-bet and is an important node of the *Ifng* gene regulatory network as illustrated by ingenuity pathway analysis (Fig. 6b). Consistently, T-bet expression was increased in Foxp3^{+} T_{reg} cells from tumors or tdLNs of B16.F10$^{\Delta Il33}$-bearing *Il33*$^{-/-}$ mice compared to wild type mice (Fig. 6c), emulated by the ST2^{+} T_{reg} cell population (Supplementary Fig. 5a). In support, T-bet expression was significantly up-regulated in T_{reg} cells infiltrating tumors of *Foxp3*^{Cre}*Il33*$^{fl/fl}$

animals compared to control *Foxp3*^{Cre} mice (Fig. 6c), while treatment of *Il33*$^{-/-}$ T_{reg} cells with recombinant IL-33 did not alter T-bet expression (Supplementary Fig. 5b).

In silico motif analysis demonstrated putative binding sites of T-bet in the regulatory region of *Ifng* locus CNS +17/+19, which presented increased accessibility in tumor-exposed IL-33-deficient T_{reg} cells (Supplementary Fig. 5c). T-bet binding to *Ifng* proximal promoter and CNS +17/+19 regions was assayed by ChIP, demonstrating significantly increased engagement (50%) in both regulatory elements of tumor-exposed *Il33*$^{-/-}$ T_{reg} cells compared to wild type (Fig. 6d). These data suggest that enhanced expression of IFN-γ in *Il33*$^{-/-}$ T_{reg} cells is facilitated by increased T-bet expression and concomitant binding to the re-arranged CNS +17/+19 regulatory region.

We then sought to assess the mechanisms underlying enhanced T-bet expression in *Il33*$^{-/-}$ Foxp3^{+} T_{reg} cells. Intracellular IL-33 has been implicated in the regulation of NF-κB signaling [17], which is required for T-bet expression [18]. Particularly, IL-33 binds to NF-κB and restricts its transcriptional activity [17]. Thus, we postulated that in the absence of intracellular IL-33, Foxp3^{+} T_{reg} cells experience increased activation of NF-κB signaling resulting in upregulation of *Tbx21* expression and IFN-γ production. In support, GO analysis of mRNAseq data highlighted the activation of NF-κB pathway in tumor-exposed *Il33*$^{-/-}$ T_{reg} cells (Supplementary Fig. 5d), while known NF-κB targets such as *Nfkbia, Nfkbid, Nfkbiz, Atf3, Fos, Jun, Gadd45b* were highly enriched among the differentially expressed genes of IL-33-deficient T_{reg} cells compared to wild type T_{reg} cells (Fig. 6e). Moreover, five of those genes (*Tnfaip3, Ifng, Cybb, Slc2a6 and Itgam*) were also unveiled by ATAC-seq data (Fig. 6e). Furthermore, NF-κB has been shown to regulate T_{reg} cell activation [19]. In accordance, intratumoral *Il33*$^{-/-}$ Foxp3^{+} T_{reg} cells exhibited an increased activation profile based on the expression of CD62L, CD44 and CD25 compared to T_{reg} cells from wild type mice (Supplementary Fig. 5e). In order to study the functional importance of the NF-κB pathway activation in T-bet and IFN-γ expression in tumor-exposed *Il33*$^{-/-}$ T_{reg} cells, we blocked NF-κB activity using IKK2 inhibitor (SC-514) in vitro. NF-κB inhibition significantly downregulated both T-bet and IFN-γ expression in Foxp3^{+} T_{reg} cells compared to untreated cells (Fig. 6f). Overall, these findings demonstrate that IFN-γ production in tumor-exposed *Il33*$^{-/-}$ Foxp3^{+} T_{reg} cells is NF-κB-T-bet axis dependent.

IL-33 deficiency potentiates the effectiveness of immunotherapy

Elucidating the molecular events that stabilize the suppressive program of tumor-specific Foxp3^{+} T_{reg} cells is of urgent need in order to advance the therapeutic potential of targeted cancer immunotherapy. Thus, B16.F10$^{\Delta Il33}$- inoculated *Il33*$^{-/-}$ and wild type mice were treated with anti-CTLA-4 or anti-PD-1. Strikingly, we observed significantly reduced tumor growth and delayed development in the *Il33*$^{-/-}$ animals treated with either anti-CTLA-4 (Fig. 7a) or anti-PD-1 (Fig. 7b) compared to non-treated littermates and to similarly treated *Il33*$^{+/+}$ animals. Both treatments did not delete intratumoral Foxp3^{+} T_{reg} cells (Fig. 7a, b) while tumor regression in anti-PD-1-treated *Il33*$^{-/-}$ and *Il33*$^{+/+}$ animals was also accompanied by a significant expansion of CD8^{+} T cells in TILs (Fig. 7b). In addition, enhanced activation of CD8^{+} T cells in *Il33*$^{-/-}$ mice was observed (Fig. 7b). In contrast,

neutralization of extracellular IL-33 (soluble ST2-sST2) together with anti-PD-1 did not show any beneficial effect on tumor regression compared to anti-PD-1 alone in wild type mice, further supporting a cell-intrinsic role of IL-33 in the effectiveness of checkpoint immunotherapy (Supplementary Fig. 6). Collectively, the impaired suppressive activity of *Il33*$^{-/-}$ Foxp3^{+} T_{reg} cells could act in concert with checkpoint inhibitor targeted immunotherapy to induce a robust tumor regression.

Discussion

An arduous task in the success of cancer immunotherapy is the selective depletion of tumor-specific Foxp3^{+} T_{reg} cells or their functional reprogramming. Identification of cell-intrinsic pathways that potentiate the suppressive program of T_{reg} cells could provide unique therapeutic strategies for tumor eradication. Herein we identify cell autonomous IL-33 to be indispensable for Foxp3^{+} T_{reg} cell function. Tumor-exposed IL-33-deficient T_{reg} cells are reprogrammed to up-regulate IFN-γ expression and exhibit decreased suppressive activity *in vivo* thus promoting tumor regression.

T_{reg} cell compartment is characterized by functional heterogeneity and lineage plasticity [20]. While, T_{reg} cell conversion is often accompanied by loss of Foxp3 expression (exT_{reg} cells), IL-33-deficient T_{reg} cells downregulate Nrp expression, produce IFN-γ and maintain Foxp3 closely resembling a "fragile" T_{reg} cell phenotype [9, 10]. In addition, IL-33-deficient T_{reg} cells exhibited increased levels of mTOR activity which has been closely correlated with T_{reg} cell instability [21, 22, 23]. Specifically, mTOR, functions through two complexes the mTOR complex 1 (mTORC1) and mTORC2 which direct suppressive function and proliferation respectively [21, 24], and we demonstrate activation of the mTORC1 complex expression in *Il33*$^{-/-}$ T_{reg} cells associated with the "fragile" phenotype of T_{reg} cells. In support ablation of autophagy [25] or loss of PTEN [22] expression in T_{reg} cells increased mTORC1 activity and led to destabilization of T_{reg} cells. Finally, enhanced mTORC1-mediated glycolytic metabolism in TRAF3IP3$^{-/-}$ T_{reg} cells caused their instability and promoted anti-tumor immunity [26].

The concept of IFN-γ expression by T_{reg} cells is not new, however its functional role remains controversial. To this end, IFN-γ-producing CD4^{+}CD127^{low}CD25^{+} T_{reg} cells are enriched in type 1 diabetes [27] and multiple sclerosis patients [28]. In addition, during T. gondii infection, T_{reg} cells, express high levels of IFN-γ and become inflammatory aiding in the clearance of the parasite [29]. Finally, *Nrp1*-deficient "fragile" Foxp3^{+} T_{reg} cells express elevated levels of IFN-γ and inhibit tumor growth [9] and T_{reg} cells deficient in the CARMA1-BCL10-MALT1 (CBM) signalosome complex up-regulate IFN-γ expression aiding the effectiveness of immunotherapy [30]. Although the molecular programs leading to induction of "fragile" IFN-γ-expressing T_{reg} cells remain ill defined, in steady state T_{reg} cells with Foxo1 nuclear exclusion [31] or with E3 ubiquitin ligase VHL deficiency [32] secrete IFN-γ and induce severe autoimmune-like inflammation. Our findings extend this knowledge demonstrating a cell-intrinsic role of IL-33 in the induction of Foxp3^{+} T_{reg} cell "fragile" phenotype during tumor immune surveillance.

Europe PMC Funders Author Manuscripts

T_{reg} cells adopt the transcriptional program of lineage specific T effector cells under inflammatory conditions [33]. In this regard, the transcription factor T-bet (*Tbx21*), which drives expression of IFN-γ [34], is expressed in a subpopulation of Foxp3$^+$ T_{reg} cells however its role remains controversial [33]. Thus, ablation of T-bet$^+$ T_{reg} cells results in the development of aggressive Th1-mediated autoimmunity [35] while genetic deletion of *Tbx21* in Foxp3$^+$ T_{reg} cells does not cause immunopathology [36]. Noticeable, T-bet expression is not always accompanied by IFN-γ production by Foxp3$^+$ T_{reg} cells [35] while in *Nrp1*$^{-/-}$ "fragile" T_{reg} cells both *Ifng* and *Tbx21* were highly expressed [9]. Our findings demonstrate major differences in chromatin accessibility of tumor exposed IL-33-deficient compared to wild type T_{reg} cells characterized by an enhanced open chromatin conformation in the CNS +17-19 flanking the *Ifng* locus of *Il33*$^{-/-}$Foxp3$^+$ T_{reg} cells, which is a known cis-regulatory element driving IFN-γ transcription [16] and permissive for T-bet binding [37]. In addition expression of *Bhlhe40*, which serves as a cofactor to regulate IFN-γ expression was significantly up-regulated in *Il33*$^{-/-}$ Foxp3$^+$$T_{reg}$ cells. Overall, IL-33 regulates the transcriptional landscape of Foxp3$^+$ T_{reg} cells in tumors through the T-bet-IFN-γ axis.

Despite its role as an alarmin, IL-33 has been shown to have a prominent role in regulating chromatin structure [38], through binding to nucleosome acidic patches composed of H2A and H2B histones [39] and also to exert transcriptional regulatory properties [40]. Of interest, IL-33 was demonstrated to interfere with the DNA-binding activity of NF-κB and to significantly impair its transcriptional activation capacity [17]. Although this finding was challenged in subsequent studies [41, 42] nevertheless a context- and cell-dependent function of IL-33 cannot be excluded. In support to data presented by Ali et al [17], we demonstrate that intracellular IL-33 acts as a "rheostat" for NF-κB activity in T_{reg} cells orchestrating their suppressive program and lineage stability. In line with this, increased NF-κB activation in T_{reg} cells was accompanied by increased IFN-γ secretion and impaired suppressive activity [43]. Although a specialized role of NF-κB subunits in T_{reg} cell stability and function through ablation of NF-κB activity in Foxp3$^+$ T_{reg} cells has been reported [19, 44], it is possible that the fine-tuning of NF-κB activity rather than its complete absence dictates the reprogramming of activated T_{reg} cells.

Unleashing the T_{reg} cell-mediated breaks without affecting immune homeostasis remains an unmet need in cancer immunotherapy. The efforts have been hampered by the lack of knowledge on the precise molecular programs that underscore T_{reg} cell function due to increased plasticity and heterogeneity of the T_{reg} cell compartment, which is also shaped by the distinct anatomic locations and inflammatory environments [20]. In the context of tumors, a major achievement would be to specifically re-program the intratumoral T_{reg} cells while their peripheral counterparts remain unaffected in order to avoid the undesired and some times life-threating immune related adverse events described during T_{reg} cell systemic ablation [45, 46]. In this regard, we reveal intracellular IL-33 as a potential "rheostat" in the lineage stability of effector T_{reg} cells in tumor-bearing animals. Importantly, IL-33 deficient mice develop a prominent response to checkpoint inhibitor immunotherapy, which is moderately effective in wild type animals [47, 48] and cancer patients [49]. In particular, consistent with previous reports [50], anti-PD-1 therapy promotes the expansion of CD8$^+$ T cell compartment in wild type and *Il33*$^{-/-}$ mice. Furthermore, it is possible that the increased activation observed in CD8$^+$ T cells may act synergistically with "fragile" T_{reg} cells to

promote tumor regression enhancing the effectiveness of immunotherapy in *Il33*$^{-/-}$ mice. Collectively these findings underscore the importance of delineating the molecular programs of T_{reg} cell stability in order to identify therapeutic targets to destabilize T_{reg} cells favoring anti-tumor immunity without ensuing autoimmunity.

Methods

Animals

C57BL/6J and *Rag1*$^{-/-}$ (C57BL/6J background) were purchased from Jackson Laboratory, *Il33*$^{-/-}$ mice (C57BL/6J background) were obtained from Amgen Inc and previously described by Martin et al. [51], *Ifng*$^{-/-}$ were purchased from Jackson Laboratory and kindly provided by E. Andreakos (Biomedical Research Foundation Academy of Athens-BRFAA), B6.129P2(SJL)-*Myd88*tm1Defx/J (*Myd88*$^{fl/fl}$) were purchased by Jackson Laboratory and kindly provided by V. Panoutsakopoulou (BRFAA), *Foxp3*^{Cre} and *Foxp3*^{gfp}.KI mice (C57BL/6 background) were kindly provided by A. Rudensky (Memorial Sloan-Kettering Cancer Center, New York, USA), *St2*$^{-/-}$ (*Il1rl1*$^{-/-}$) mice were kindly provided by AN. McKenzie (Medical Research Council Laboratory of Molecular Biology, Cambridge, UK) and *Il33*$^{fl/fl}$ mice were purchased from Jackson Laboratory. *Il33*$^{-/-}$*Foxp3*^{gfp} mice were generated by crossing *Il33*$^{-/-}$ mice with *Foxp3*^{gfp}.KI mice, *Il33*$^{-/-}$*Ifng*$^{-/-}$ mice by crossing *Il33*$^{-/-}$ with *Ifng*$^{-/-}$, *Foxp3*^{Cre}*Myd88*$^{fl/fl}$ mice by crossing *Foxp3*^{Cre} with *Myd88*$^{fl/fl}$ and *Foxp3*^{Cre}*Il33*$^{fl/fl}$ by crossing *Foxp3*^{Cre} with *Il33*$^{fl/fl}$. All mice were maintained in the animal facility of BRFAA. All procedures were in accordance to institutional guidelines and were approved by the Institutional Committee of Protocol Evaluation in conjunction with the Directorate of Agriculture and Veterinary Policy, Region of Attika, Greece (1202/19.03.2018). Unless otherwise indicated, experiments used sex- and age-matched mice between 6 and 12 weeks of age.

Cell lines

The cancer cell lines B16.F10 and LLC were kindly provided by A. Eliopoulos (School of Medicine, University of Crete, Greece) and were negative for mycoplasma, tested by PCR.

Transplant tumor models

Transplant tumor models were performed as described previously [52]. Mice were implanted subcutaneously (s.c.) on the back with 3×10^5 B16.F10 melanoma cells or shIL-33 transduced B16.F10 cells (B16.F10$^{\Delta Il33}$) or LLC cells. For the application of immunotherapy or the depletion of T_{reg} cells every three days following the implantation, mice were treated with anti-CTLA-4 (clone 4F10, Bioceros LB) (100 μg/ 100 μl/ intraperitoneally-i.p. in each mouse) or anti-PD-1 (clone RMP1-14 Bioceros LB) (200 μg/ 100 μl i.p./ mouse) or anti-CD25 (clone PC61, Bioceros LB) (100 μg/ 100 μl i.p. / mouse). For the adoptive transfer experiments 3×10^5 $CD4^+CD25^+GITR^+Foxp3^+$ cells sorted highly pure (98%) from magnetically-CD4-enriched LN and spleen cells of naïve C57BL/6 or *Il33*$^{-/-}$ or *Ifng*$^{-/-}$ or *Il33*$^{-/-}$*Ifng*$^{-/-}$ or *St2*$^{-/-}$ mice were intravenously transferred to *Rag1*$^{-/-}$ hosts with 8×10^5 $CD4^+CD25^-GITR^-$ cells and 7×10^5 $CD8^+$ cells sorted highly pure (96%) from LNs and spleen of naïve C57BL/6 mice. Three days later *Rag1*$^{-/-}$ mice were implanted with B16.F10$^{\Delta il3}$ cells. Tumors were measured every day by caliper, and tumor

Europe PMC Funders Author Manuscripts

Europe PMC Funders Author Manuscripts

volume was calculated as 0.5 × length × width × width. Mice were euthanized when tumors grew larger than 1,100 mm^3. At the endpoint of each experiment tumor weight was also determined.

Lentivirus production and B16.F10 transduction

To knockdown the expression of *Il33* we designed 2 shRNA sequences (shIL-33_1: 5′-GGTGCTACTACGCTACTATGA-3′ and shIL-33_2: 5′-GAACATGAGTCCCATCAAAGA-3′) that specifically target the transcripts of mouse *Il33*. The shRNA sequences were cloned into the pLKO.1 lentiviral vector. HEK 293T (kindly provided by A. Klinakis) were transiently co-transfected with plasmids containing the viral packaging genes (pMDG and R891) and with pLKO.1 carrying either the shIL-33 or an shRNA scramble sequence. Lentivirus-containing medium was collected at 24 post-transfection and used to transduce B16.F10 cells for 16 h. Two days later selection of transduced cells was started with puromycin (5 μg/ml) or blasticidin (5 μg/ml), for 5 and 12 days, respectively. A pLKO vector carrying the *GFP* gene was used to assess transduction efficiency and the titer according to the manufacturer's instructions.

Cell isolation from tumors and lymphoid organs

Single cell suspensions from LNs, spleens and thymus were generated by passing them through a 40 μm cell strainer. BM cells were isolated by flushing out femur and tibia. TILs were isolated by dissociating tumor tissue in the presence of collagenase D (1 mg/ml, Roche) and DNAse I (0.25 mg/ml, Sigma) for 45 min before passing through a 40 μm cell strainer. For LN cells activation, 4×10^5 total tdLN cells were cultured with Dynabeads™ mouse T-activator CD3/CD28 (Gibco) in a ratio 1:1 for 48 h. Recombinant murine IL-2 (1000 U/ml, Peprotech) and recombinant murine IL-33 (20 ng/ml, Immunotools) were added where indicated.

Flow cytometry

For staining of extracellular markers, cell suspensions were incubated with antibodies for 20 min at 4°C. The following antibodies were used (all antibodies were purchased from BioLegend): CD45 (clone 30-F11), CD4 (RM4-4), CD8 (53-6.7), CD11c (N418), CD11b (M1/70), NK1.1 (PK136), IAb (AF6-120.1), CD25 (PC61), GITR (DTA-1), KLRG-1 (2F1/KLRG1), OX-40 (OX-86), CTLA-4 (UC10-4B9), LAG-3 (C9B7W), ICOS (7E.17G9), PD-1, CD44 (IM7), CD62L (MEL-14), NRP (3E12), ST2 (DIH9), Ki67 (16A8), pγH2AX (2F3). For Foxp3 (150D), phospho-mTOR (Ser2448) (MRRBY), phospho-S6 (Ser235, Ser236) (cupk43k), phospho-4E-BP1(T36/T45) (V3NTY24) and T-bet (4B10) intracellular staining, cells were stained for the extracellular markers and then fixed and stained using the Foxp3 Staining Set (eBioscience) according to the vendor instructions. For IFN-γ (XMG1.2) intracellular staining, cells were incubated with 50 ng/ml PMA (Sigma-Aldrich), 2 μg/ml Ionomycin (Sigma-Aldrich) and Brefeldin (1/1000) (BD) for 4 h at 37°C and 5% CO2, stained for extracellular markers, fixed and stained using the Foxp3 Staining Set (eBioscience). All samples were analyzed with ARIA III (BD). Flow cytometry data were analyzed with FlowJo 8.7 and vX0.7 software.

Quantitative PCR

Cells RNA was extracted using Macherey Nagel Nucleospin RNA kit and Nucleospin RNA XS kit according to manufacturer guidelines. First-strand cDNA synthesis was performed using PrimeScript™ RT reagent kit (Takara). qPCR was carried out in 20 μl reactions using the KAPA SYBR@ FAST (KapaBiosystems). The program used was: 95°C for 3 min, 95°C for 10 sec and 62°C for 30 sec for 40 cycles. Relative expression of target genes was calculated by comparing them to the expression of the house-keeping genes *Hprt*. The following primers were used:

Hprt: Forward 5′-GTGAAACTGGAAAAGCCAAA-3′, Reverse 5′-GGACGCAGCAACTGACAT-3′, *Il33*: Forward 5′-GCTGCGTCTGTTGACACATT-3′, Reverse 5′-CACCTGGTCTTGCTCTTGGT-3′, *Ifng*: Forward 5′-ATGAACGCTACACACTGCATC-3', Reverse 5'-CCATCCTTTTGCCAGTTCCTC-3′ from Invitrogen.

ELISA

Tumor and LN homogenates were generated in phosphate buffered saline (PBS) containing a cocktail of protease inhibitors (Roche) using a pestle. B16.F10 transduced with scramble, B16.F10 transduced with shIL-33_1 and B16.F10 transduced with shil33_2 lysates were generated by 5 freeze-thaw cycles of cultured cells. The homogenates and lysates were centrifuged and used for IL-33 ELISA (R&D) according to manufacturer's guidelines.

Immunohistochemistry

Tumor samples were fixed overnight in 4% PFA/PBS, washed with PBS and a small part was immersed in 30% sucrose/PBS, embedded in OCT (VWR Chemicals) and frozen, while the rest was embedded in paraffin. 4-μm-thick sections of FFPE (Formalin-Fixed, Paraffin-Embedded) tumors were blocked using 1% BSA in TBS containing 0.05% Tween 20 (Sigma) (TTBS) and incubated with anti-Ki67 (Thermofisher Scientific, MA5-14520) or anti-CD31 (Abcam, ab28364) primary antibodies. A biotinylated secondary anti-rabbit antibody (Vector Laboratories) and the Vectastain ABC kit (Vector Laboratories) were used for signal detection and amplification, respectively. Signal development was performed with the Vectastain DAB (3,3-diamino-benzidine) kit (Vector Laboratories) and hematoxylin was used as a counterstain. Images were acquired with an Eclipse E800 microscope (Nikon) equipped with a QImaging Digital Camera. Cryosections were incubated with the anti-CD31 and anti-VCAM1 (Abcam, ab19569) antibodies, followed by the secondary A568-conjugated anti–rabbit antibody (Invitrogen, A110011) and the A488-conjugated anti-rat antibody (Invitrogen, A11006), respectively. Mounting medium containing DAPI (Sigma-Aldrich) was used to stain the nuclei and images were acquired using a Leica TCS SP8X White Light Laser confocal system. Quantifications were performed using ImageJ software analysis

mRNAseq and Microarray data

Microarray data generated by TCGA were downloaded from TCGA data portal (https://tcga-data.nci.nih.gov/tcga/).

The library preparation for mRNAseq was carried out in the Greek Genome Center (GGC) of BRFAA. RNA was collected from $CD4^+CD25^+GITR^+Foxp3^+$ sorted cells from tdLNs. RNA-seq libraries (GSE138871) were prepared using the TruSeq RNA kit using 500 ng of total RNA. The libraries were constructed according to Illumina's protocols and then were mixed in equal amounts. Paired-end 38 bp reads for 6 samples were generated with NextSeq500 in the GGC. RNA-seq analysis was done using in-house developed sub-pipeline [53]. Specifically, sequencing reads of sgRNA knockdown samples and their control samples aligned to reference genome mm10 using STAR-aligner version 2.4.2 [54] with parameters suggested by TCGA expression mRNA-seq pipeline(https://docs.gdc.cancer.gov/Data/Bioinformatics_Pipelines/Expression_mRNA_Pipeline/), and the raw read counts were generated. Then DESeq2 [55] was used to perform differential expression analysis.

Assay for Transposase Accessible Chromatin (ATAC)-Sequencing

ATAC-seq was performed as described previously [56]. In brief, $2 \times 10^4 – 6 \times 10^4$ T_{reg} cells from tdLNs were sorted as $CD4^+CD25^+GITR^+Foxp3^+$ using the BD AriaII. Cells were resuspended in 50 μl cold lysis buffer (10 mM Tris-HCl, pH 7.4, 10 mM NaCl, 3 mM $MgCl_2$, 0,1% IGEPAL CA-630) and centrifuged at 500 g for 10 min. After centrifugation supernatant was aspirated and transposition was performed with in-house Tn5 Transposase in 20 μl tagmentation buffer (10 mM TAPS-NaOH, pH8.5, 5 mM MgCl2, 10% DMF) for 30 min at 37°C. DNA was purified using the Qiagen MinElute Kit (Qiagen) and amplified using the NEBNext High-Fidelitiy PCR Master Mix (New England BioLabs) and customized Nextera PCR primers:

Ad1_noMX	5′AATGATACGGCGACCACCGAGATCTACACTCGTCGGCAGCGTCAGATGTG′3
Ad2.1_TAAGGCGA	5′CAAGCAGAAGACGGCATACGAGATTCGCCTTAGTCTCGTGGGCTCGGAGATGT′3
Ad2.3_AGGCAGAA	5′CAAGCAGAAGACGGCATACGAGATTTCTGCCTGTCTCGTGGGCTCGGAGATGT′3
Ad2.4_TCCTGAGC	5′CAAGCAGAAGACGGCATACGAGATGCTCAGGAGTCTCGTGGGCTCGGAGATGT′3
Ad2.8_CAGAGAGG	5′CAAGCAGAAGACGGCATACGAGATCCTCTCTGGTCTCGTGGGCTCGGAGATGT′3
Ad2.9_GCTACGCT	5′CAAGCAGAAGACGGCATACGAGATAGCGTAGCGTCTCGTGGGCTCGGAGATGT′3
Ad2.10_CGAGGCTG	5′CAAGCAGAAGACGGCATACGAGATCAGCCTCGGTCTCGTGGGCTCGGAGATGT′3
Ad2.13_GTCGTGAT	5′CAAGCAGAAGACGGCATACGAGATATCACGACGTCTCGTGGGCTCGGAGATGT′3
Ad2.14_ACCACTGT	5′CAAGCAGAAGACGGCATACGAGATACAGTGGTGTCTCGTGGGCTCGGAGATGT′3
Ad2.15_TGGATCTG	5′CAAGCAGAAGACGGCATACGAGATCAGATCCAGTCTCGTGGGCTCGGAGATGT′3

Libraries were purified using the Qiagen MinElute Kit (Qiagen) and quality checked using the Agilent Tapestation 2200. Libraries were sequenced on an Illumina HiSeq1500 with a minimum of 10×10^6 reads/sample (GSE138872). ATAC-seq analysis was done using in-house developed sub-pipeline [53]. Specifically, sequencing reads were aligned to reference genome mm10 using sing Botwie2 [57] with default parameter. MACS2 [58] is used for peak calling with broad peak calling mode. DiffBind is used to perform differential binding analysis with EDGER normalization method, and q-value of 0.05 was used as the cutoff for calling differential binding peaks.

Pyrosequencing

1×10^5-1×10^6 T effectors ($CD4^+CD25^-GITR^-Foxp3^-$) and T_{reg} cells ($CD4^+CD25^+GITR^+Foxp3^+$) were sorted from tdLNs and their DNA was isolated using Nucleospin Tissue (Macherey Nagel) according to manufacturer's guidelines. Sodium bisulfite treatment of genomic DNA was carried out using the EZ DNA Methylation Gold Kit (Zymo research) according to the manufacturer´s instructions. Fragments for pyrosequencing were generated by PCR using the PyroMark PCR Kit (Qiagen) with the following protocol denaturation at 95°C for 15 min, followed by 44 cycles at 94°C for 30 s, 56°C for 30 s, and 72°C for 30 s. PCR products were visualized by gel electrophoresis. The primers used were: SET1: Forward 5′-GGAGGAGGAAGAGGAGGT-3′, Reverse 5′-AAATATAAACACCAAATAAAACCC-3′, Sequencing 5′-GGAGGAAGAGGAGGTT-3′ and SET2: Forward 5′-GAAGAGGTTTTGGGGTTGT-3′, Reverse 5′-CCATCCTCTTCCTCATCAAC-3′ and Sequencing 5′-AGGTTTTGGGGTTGTTT-3′. For purification of biotinylated fragment, 20 μl of PCR products were added to a mix consisting of 3 μl Streptavidin Sepharose HP™ Beads (GE Healthcare) and 40 μl binding buffer (QIAGEN). Sepharose beads with the single-stranded templates attached were added to a 24 well Plate (QIAGEN) containing a mix of 25 μl annealing buffer (QIAGEN) and 0.3 μM of the corresponding sequencing primers (Invitrogen). Pyrosequencing was performed in a PyroMark Q24 Instrument with the PyroMark Gold Q24 Reagent Kit (QIAGEN). For pyrogram exposure including CpG-site methylation calculation, the PyroMark Q24 Method 010 Software Version 2.0.7 (QIAGEN) was applied. Only pyrograms including sharp peaks with sufficient height for each injected nucleotide of interest and without peaks for unsuccessful bisulfite treatment or background controls were considered.

Chromatin immunoprecipitation (ChIP)

2×10^6 cells were cross-linked with 1% (vol/vol) formaldehyde for 10 min at 25 °C (followed by extensive wash with PBS) and lysed with 120 μl lysis buffer (1% (wt/vol) SDS, 10 mM EDTA and 50 mM Tris-HCl, pH 8.1, 1 × protease inhibitor 'cocktail' (Roche), 1 mM PMSF). Chromatin is sheared by Covaris Sonicator System to 200-400 bp fragments. Supernatants are collected after centrifugation and diluted at least 5 volumes in Dilution Buffer (1% (vol/vol) Triton X-100, 2 mM EDTA, 150 mM NaCl and 20 mM Tris-HCl, pH 8.1). Antibody (2 μg) is incubated with diluted chromatin overnight, after preclearing. Immunoprecipitation continues by incubation with protein G Dynal magnetic beads (Invitrogen) for at least 3 h at 4°C. Magnetic bead– immunoprecipitated chromatin complexes are then washed 8 times with High Salt Wash Buffer (2 times), Low Salt Wash Buffer (2 times), LiCl Wash Buffer (2 times) and TE Buffer (2 times). Immunoprecipitated chromatin is then eluted from Magnetic beads with Proteinase K Digestion Buffer and heated at 65 °C for at least 6 h for reversal of the formaldehyde crosslinking. DNA fragments are purified with NucleoMag beads kit (MN) and analyzed by SYBR Green Quantitative Real-time PCR. The following antibody was used for ChIP: anti-mouse T-bet (4B10). The following primer pair was used for ChIP: Forward 5′-GCTGTCTCATCGTCAGAGAG-3′, Reverse 5′-GATGGTGACAGATAGGTGGG-3′.

Targeted proteomics

The Skyline software was used for selecting nine proteotypic peptides for IL-33 along with the m/z values of the precursor ions and specific fragment ions. These nine precursor ions were selected for detection by PRM. The samples were processed with the GeLC-MS sample preparation protocol [59]. Specifically, cell pellets were homogenized in 100 μL of lysis buffer (7 M Urea, 2 M Thiourea, 4% w/v CHAPS, 1% w/v DTE) and the protein concentration was determined by the Bradford assay. Subsequently, 10 μg of protein per sample were loaded on SDS-PAGE wells and the electrophoresis was stopped when the samples entered the resolving gel. Gels were stained with Coomassie colloidal blue and a single band containing all proteins was excised. In gel reduction and alkylation was followed by trypsin digestion in 0.01 M ammonium bicarbonate pH 8.5. Peptides were extracted from the gel bands, dried in a vacuum centrifuge and re-suspended in 10 μL 0.1% v/v formic acid, pH 3.5. Analysis of the extracted peptides was performed with an UltiMate 3000 Nano HPLC Dionex Ultimate® 3000 RSLS system (Dionex™; Thermo Fisher Scientific, Inc.) coupled to a Q Exactive (Thermo Fisher Scientific, Inc) mass spectrometer operating in PRM mode. A volume of 5 μL was injected into the chromatography system and peptides were fractionated in a C18 column during a 70 min run (0.3 μL/min flow rate) using a gradient of up to 80% v/v Acetonitrile for elution. The MS2 parameters were: resolution 35,000 and injection time (IT) 128 ms. The PRM data files were analyzed using the Skyline software. All the acquired data were inspected and processed manually.

Data analysis and statistics

Results are presented as mean ± s.d. Data were analyzed by two-tailed Student's t-test or two-tailed Mann–Whitney U-test, as appropriate (after testing for normality with the F-test). Multiple-group comparisons were performed using one-way analysis of variance (ANOVA) and the Dunnett's or Tukey's multiple comparison tests. Kaplan Meier statistics were evaluated by Log rank test. All statistical analyses were performed on GraphPad Prism 5 and 8.2.1 software. P values < 0.05 were considered to be statistically significant.

Supplementary Material

Refer to Web version on PubMed Central for supplementary material.

Acknowledgements

We thank T. Alissafi for fruitful conversations and critical reading of the manuscript, R. M. Barouni for its technical assistance, P. Alexakos for his technical assistance on animal handling and maintenance, A. Apostolidou for her technical assistance on flow cytometry and cell sorting. We also thank M. Makridakis and G. Kontostathi for PRM analysis. This work was supported by grants from the Greek General Secretariat of Research and Technology (Aristeia II 3468 to P.V.). M.B. was funded by the German Research Foundation (BE 4427/3-1) and is a member of the excellence cluster ImmunoSensation. T.C. was supported by the ERC (DEMETINL-683145) and the German Research Foundation (SFB 1181). D.B. was supported by the ERC under the European Union's Horizon 2020 research and innovation programme (grant agreement No 742390). A.Ha. is supported by IKY Fellowships of Excellence for Postgraduate Studies in Greece, Siemens Programme and by "Stratigos" grant of the Hellenic Society of Melanoma Study. A.B. is financed by Greece and the European Union (European Social Fund-ESF) through the Operational Programme «Human Resources Development, Education and Lifelong Learning» in the context of the project "Reinforcement of Postdoctoral Researchers" (MIS-5001552), implemented by the State Scholarships Foundation (IKY). D.B. and P.V. were supported by the European Union's Horizon 2020 research and innovation programme under grant agreement No 733100.

Europe PMC Funders Author Manuscripts

References

1. Sakaguchi S, Yamaguchi T, Nomura T, Ono M. Regulatory T cells and immune tolerance. Cell. 2008; 133:775–787. [PubMed: 18510923]
2. Hatziioannou A, Alissafi T, Verginis P. Myeloid-derived suppressor cells and T regulatory cells in tumors: unraveling the dark side of the force. J Leukoc Biol. 2017; 102:407–421. [PubMed: 28360184]
3. Zou W. Regulatory T cells, tumour immunity and immunotherapy. Nat Rev Immunol. 2006; 6:295–307. [PubMed: 16557261]
4. Abdel-Wahab N, Shah M, Suarez-Almazor ME. Adverse Events Associated with Immune Checkpoint Blockade in Patients with Cancer: A Systematic Review of Case Reports. PLoS One. 2016; 11:e0160221. [PubMed: 27472273]
5. Jenkins RW, Barbie DA, Flaherty KT. Mechanisms of resistance to immune checkpoint inhibitors. Br J Cancer. 2018; 118:9–16. [PubMed: 29319049]
6. Liew FY, Girard JP, Turnquist HR. Interleukin-33 in health and disease. Nat Rev Immunol. 2016; 16:676–689. [PubMed: 27640624]
7. Cayrol C, Girard JP. Interleukin-33 (IL-33): A nuclear cytokine from the IL-1 family. Immunol Rev. 2018; 281:154–168. [PubMed: 29247993]
8. Schiering C, et al. The alarmin IL-33 promotes regulatory T-cell function in the intestine. Nature. 2014; 513:564–568. [PubMed: 25043027]
9. Overacre-Delgoffe AE, et al. Interferon-gamma Drives Treg Fragility to Promote Anti-tumor Immunity. Cell. 2017; 169:1130–1141 e1111. [PubMed: 28552348]
10. Overacre-Delgoffe AE, Vignali DAA. Treg Fragility: A Prerequisite for Effective Antitumor Immunity? Cancer Immunol Res. 2018; 6:882–887. [PubMed: 30068755]
11. Andersson P, et al. Molecular mechanisms of IL-33-mediated stromal interactions in cancer metastasis. JCI Insight. 2018; 3:e122375.
12. Setiady YY, Coccia JA, Park PU. In vivo depletion of CD4+FOXP3+ Treg cells by the PC61 anti-CD25 monoclonal antibody is mediated by FcgammaRIII+ phagocytes. Eur J Immunol. 2010; 40:780–786. [PubMed: 20039297]
13. Braun H, Afonina IS, Mueller C, Beyaert R. Dichotomous function of IL-33 in health and disease: From biology to clinical implications. Biochem Pharmacol. 2018; 148:238–252. [PubMed: 29309756]
14. Toker A, et al. Active demethylation of the Foxp3 locus leads to the generation of stable regulatory T cells within the thymus. J Immunol. 2013; 190:3180–3188. [PubMed: 23420886]
15. Zeng H, et al. mTORC1 couples immune signals and metabolic programming to establish T(reg)-cell function. Nature. 2013; 499:485–490. [PubMed: 23812589]
16. Balasubramani A, et al. Modular utilization of distal cis-regulatory elements controls Ifng gene expression in T cells activated by distinct stimuli. Immunity. 2010; 33:35–47. [PubMed: 20643337]
17. Ali S, et al. The dual function cytokine IL-33 interacts with the transcription factor NF-kappaB to dampen NF-kappaB-stimulated gene transcription. J Immunol. 2011; 187:1609–1616. [PubMed: 21734074]
18. Lin L, Spoor MS, Gerth AJ, Brody SL, Peng SL. Modulation of Th1 activation and inflammation by the NF-kappaB repressor Foxj1. Science. 2004; 303:1017–1020. [PubMed: 14963332]
19. Grinberg-Bleyer Y, et al. NF-kappaB c-Rel Is Crucial for the Regulatory T Cell Immune Checkpoint in Cancer. Cell. 2017; 170:1096–1108 e1013. [PubMed: 28886380]
20. Hori S. Lineage stability and phenotypic plasticity of Foxp3(+) regulatory T cells. Immunol Rev. 2014; 259:159–172. [PubMed: 24712465]
21. Apostolidis SA, et al. Phosphatase PP2A is requisite for the function of regulatory T cells. Nat Immunol. 2016; 17:556–564. [PubMed: 26974206]
22. Huynh A, et al. Control of PI(3) kinase in Treg cells maintains homeostasis and lineage stability. Nat Immunol. 2015; 16:188–196. [PubMed: 25559257]

23. Delgoffe GM, et al. The kinase mTOR regulates the differentiation of helper T cells through the selective activation of signaling by mTORC1 and mTORC2. Nat Immunol. 2011; 12:295–303. [PubMed: 21358638]
24. Shrestha S, et al. Treg cells require the phosphatase PTEN to restrain TH1 and TFH cell responses. Nat Immunol. 2015; 16:178–187. [PubMed: 25559258]
25. Wei J, et al. Autophagy enforces functional integrity of regulatory T cells by coupling environmental cues and metabolic homeostasis. Nat Immunol. 2016; 17:277–285. [PubMed: 26808230]
26. Yu X, et al. Metabolic control of regulatory T cell stability and function by TRAF3IP3 at the lysosome. J Exp Med. 2018; 215:2463–2476. [PubMed: 30115741]
27. McClymont SA, et al. Plasticity of human regulatory T cells in healthy subjects and patients with type 1 diabetes. J Immunol. 2011; 186:3918–3926. [PubMed: 21368230]
28. Dominguez-Villar M, Baecher-Allan CM, Hafler DA. Identification of T helper type 1-like, Foxp3+ regulatory T cells in human autoimmune disease. Nat Med. 2011; 17:673–675. [PubMed: 21540856]
29. Oldenhove G, et al. Decrease of Foxp3+ Treg cell number and acquisition of effector cell phenotype during lethal infection. Immunity. 2009; 31:772–786. [PubMed: 19896394]
30. Di Pilato M, et al. Targeting the CBM complex causes Treg cells to prime tumours for immune checkpoint therapy. Nature. 2019; 570:112–116. [PubMed: 31092922]
31. Ouyang W, et al. Novel Foxo1-dependent transcriptional programs control T(reg) cell function. Nature. 2012; 491:554–559. [PubMed: 23135404]
32. Lee JH, Elly C, Park Y, Liu YC. E3 Ubiquitin Ligase VHL Regulates Hypoxia-Inducible Factor-1alpha to Maintain Regulatory T Cell Stability and Suppressive Capacity. Immunity. 2015; 42:1062–1074. [PubMed: 26084024]
33. Koch MA, et al. The transcription factor T-bet controls regulatory T cell homeostasis and function during type 1 inflammation. Nat Immunol. 2009; 10:595–602. [PubMed: 19412181]
34. Szabo SJ, et al. A novel transcription factor, T-bet, directs Th1 lineage commitment. Cell. 2000; 100:655–669. [PubMed: 10761931]
35. Levine AG, et al. Stability and function of regulatory T cells expressing the transcription factor T-bet. Nature. 2017; 546:421–425. [PubMed: 28607488]
36. Yu F, Sharma S, Edwards J, Feigenbaum L, Zhu J. Dynamic expression of transcription factors T-bet and GATA-3 by regulatory T cells maintains immunotolerance. Nat Immunol. 2015; 16:197–206. [PubMed: 25501630]
37. Sekimata M, et al. CCCTC-binding factor and the transcription factor T-bet orchestrate T helper 1 cell-specific structure and function at the interferon-gamma locus. Immunity. 2009; 31:551–564. [PubMed: 19818655]
38. Zhou J, Fan JY, Rangasamy D, Tremethick DJ. The nucleosome surface regulates chromatin compaction and couples it with transcriptional repression. Nat Struct Mol Biol. 2007; 14:1070–1076. [PubMed: 17965724]
39. Roussel L, Erard M, Cayrol C, Girard JP. Molecular mimicry between IL-33 and KSHV for attachment to chromatin through the H2A-H2B acidic pocket. EMBO Rep. 2008; 9:1006–1012. [PubMed: 18688256]
40. Carriere V, et al. IL-33, the IL-1-like cytokine ligand for ST2 receptor, is a chromatin-associated nuclear factor in vivo. Proc Natl Acad Sci U S A. 2007; 104:282–287. [PubMed: 17185418]
41. Choi YS, et al. Nuclear IL-33 is a transcriptional regulator of NF-kappaB p65 and induces endothelial cell activation. Biochem Biophys Res Commun. 2012; 421:305–311. [PubMed: 22708120]
42. Travers J, et al. Chromatin regulates IL-33 release and extracellular cytokine activity. Nat Commun. 2018; 9
43. Polesso F, Sarker M, Anderson A, Parker DC, Murray SE. Constitutive expression of NF-kappaB inducing kinase in regulatory T cells impairs suppressive function and promotes instability and pro-inflammatory cytokine production. Sci Rep. 2017; 7

44. Oh H, et al. An NF-kappaB Transcription-Factor-Dependent Lineage-Specific Transcriptional Program Promotes Regulatory T Cell Identity and Function. Immunity. 2017; 47:450–465 e455. [PubMed: 28889947]
45. Kim JM, Rasmussen JP, Rudensky AY. Regulatory T cells prevent catastrophic autoimmunity throughout the lifespan of mice. Nat Immunol. 2007; 8:191–197. [PubMed: 17136045]
46. Alissafi T, Hatzioannou A, Legaki AI, Varveri A, Verginis P. Balancing cancer immunotherapy and immune-related adverse events: The emerging role of regulatory T cells. J Autoimmun. 2019:102310. [PubMed: 31421963]
47. Liu Z, et al. Modifying the cancer-immune set point using vaccinia virus expressing re-designed interleukin-2. Nat Commun. 2018; 9
48. Ishizuka JJ, et al. Loss of ADAR1 in tumours overcomes resistance to immune checkpoint blockade. Nature. 2019; 565:43–48. [PubMed: 30559380]
49. Postow MA, Callahan MK, Wolchok JD. Immune Checkpoint Blockade in Cancer Therapy. J Clin Oncol. 2015; 33:1974–1982. [PubMed: 25605845]
50. Wei SC, et al. Distinct Cellular Mechanisms Underlie Anti-CTLA-4 and Anti-PD-1 Checkpoint Blockade. Cell. 2017; 170:1120–1133 e1117. [PubMed: 28803728]
51. Martin P, et al. Disease severity in K/BxN serum transfer-induced arthritis is not affected by IL-33 deficiency. Arthritis Res Ther. 2013; 15:R13. [PubMed: 23324173]
52. Hatzioannou A, et al. Intratumoral accumulation of podoplanin-expressing lymph node stromal cells promote tumor growth through elimination of CD4(+) tumor-infiltrating lymphocytes. Oncoimmunology. 2016; 5:e1216289. [PubMed: 27757315]
53. Gong Y, et al. lncRNA-screen: an interactive platform for computationally screening long non-coding RNAs in large genomics datasets. BMC Genomics. 2017; 18:434. [PubMed: 28583068]
54. Dobin A, et al. STAR: ultrafast universal RNA-seq aligner. Bioinformatics. 2013; 29:15–21. [PubMed: 23104886]
55. Love MI, Huber W, Anders S. Moderated estimation of fold change and dispersion for RNA-seq data with DESeq2. Genome Biol. 2014; 15:550. [PubMed: 25516281]
56. Buenrostro JD, Giresi PG, Zaba LC, Chang HY, Greenleaf WJ. Transposition of native chromatin for fast and sensitive epigenomic profiling of open chromatin, DNA-binding proteins and nucleosome position. Nat Methods. 2013; 10:1213–1218. [PubMed: 24097267]
57. Langmead B, Salzberg SL. Fast gapped-read alignment with Bowtie 2. Nat Methods. 2012; 9:357–359. [PubMed: 22388286]
58. Zhang Y, et al. Model-based analysis of ChIP-Seq (MACS). Genome Biol. 2008; 9:R137. [PubMed: 18798982]
59. Makridakis M, Vlahou A. GeLC-MS: A Sample Preparation Method for Proteomics Analysis of Minimal Amount of Tissue. Methods Mol Biol. 2018; 1788:165–175. [PubMed: 28994030]

Europe PMC Funders Author Manuscripts

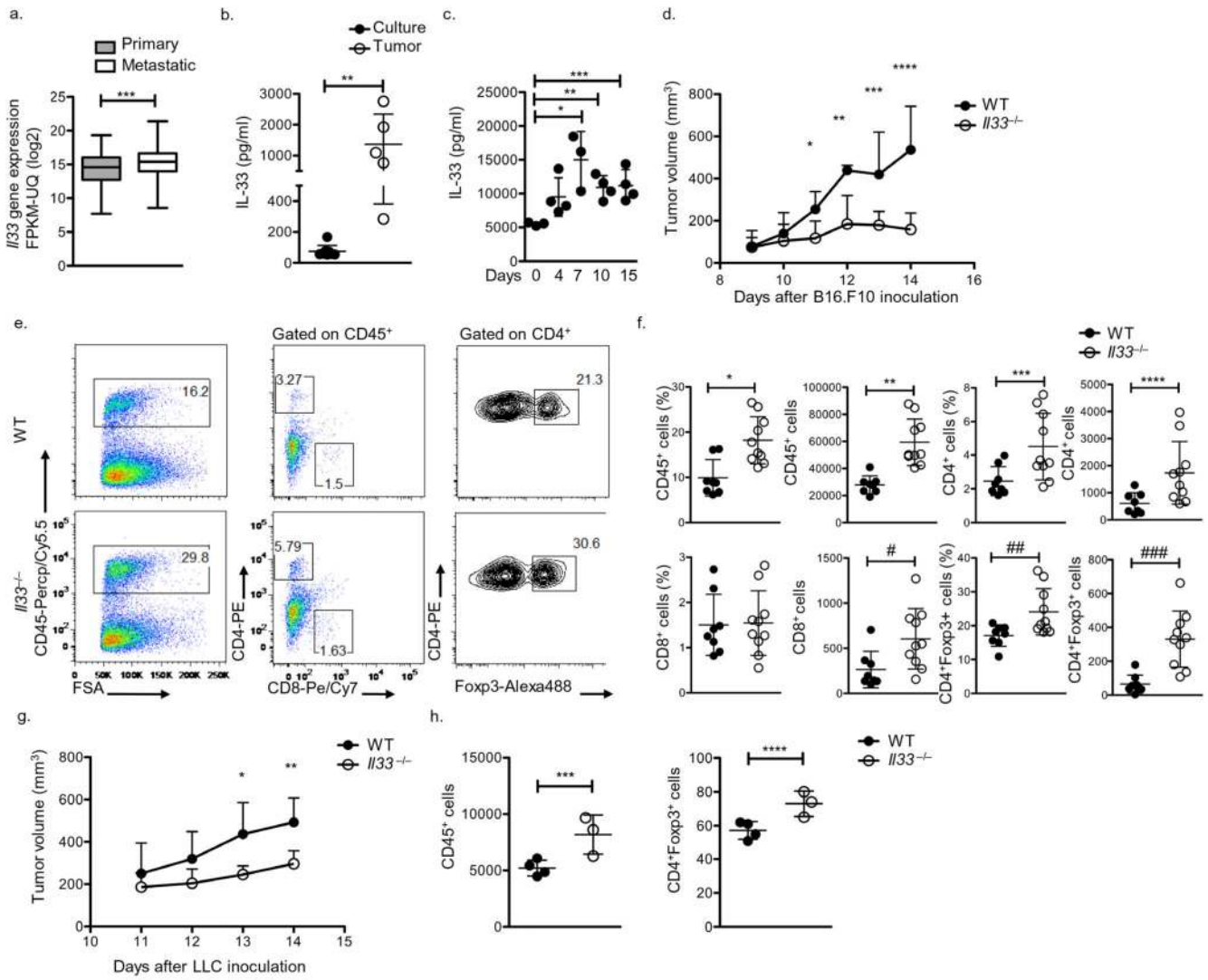

Figure 1. IL-33 deficiency promotes anti-tumor immunity and inhibits tumor growth.

(a) Whiskers plot (min to max) of IL-33 expression levels (FPKM-UQ) based on TCGA datasets of primary (n=102 biologically independent human samples) and metastatic SCKM (n=367 biologically independent human samples), ***P=0.0006 (b) IL-33 levels (pg/ml) in homogenates of cultured B16.F10 melanocytes (n=8, biological independent cell cultures) and tumors from day 14 B16.F10 inoculated WT mice (n=5) determined by ELISA, **P=0.0016 (c) IL-33 levels (pg/ml) in tdLNs homogenates from B16.F10-inoculated mice at indicated time points (day 0 n=3, day 4 n=4, day 7=3, day 10=4, day 15=4), *P=0.00195, **P=0.049, ***P=0.039 (d) Tumor volume (mm^3) curve of WT (n=8) and *Il33*$^{-/-}$ (n=10) mice following B16.F10 inoculation. *P=0.003, **P=0.0025, ***P=0.0027, ****P=0.0001. Gating strategy (e), percentages and numbers per 5×10^5 tumor cells (f) of intratumoral $CD45^+$ cells, $CD4^+$, $CD8^+$ and $CD4^+Foxp3^+$ T cells on day 14 after B16.F10 inoculation of WT (n=8) and *Il33*$^{-/-}$ (n=10) mice. Numbers denote percentages of gated populations. *P=0.0019, **P<0.0001, ***P=0.02, ****P=0.0117, N.S.=0.9076, $^{\#}$P=0.0267, $^{\#\#}$P=0.0173, $^{\#\#\#}$P=0.0002 (g) Tumor volume (mm^3) curve of WT (n=4) and *Il33*$^{-/-}$ (n=3) mice following

Europe PMC Funders Author Manuscripts

LLC inoculation. *P=0.0255, **P=0.0445 (h) Numbers per 5×10^5 tumor cells of intratumoral $CD45^+$ and $CD4^+Foxp3^+$ T cells on day 14 after LLC inoculation of WT (n=4) and *Il33*$^{-/-}$ (n=3) mice. ***P=0.0245, ****P=0.0214. Data are shown as means ± SD. Representative data from three (g, h) and four (c, e, f) independent experiments. (a, f*, f$^{\#}$, f$^{\#\#}$, h) unpaired two-tailed t-test, (b, f**, f***, f****, f$^{\#\#\#}$) Mann-Whitney two-tailed U-test, (c) one-way ANOVA with Dunnett's multiple comparisons test, (d, g) multiple unpaired two-tailed t-tests between WT and *Il33*$^{-/-}$ at each time point. (c, d, e, f, g, h) n=biologically independent mouse samples.

Europe PMC Funders Author Manuscripts

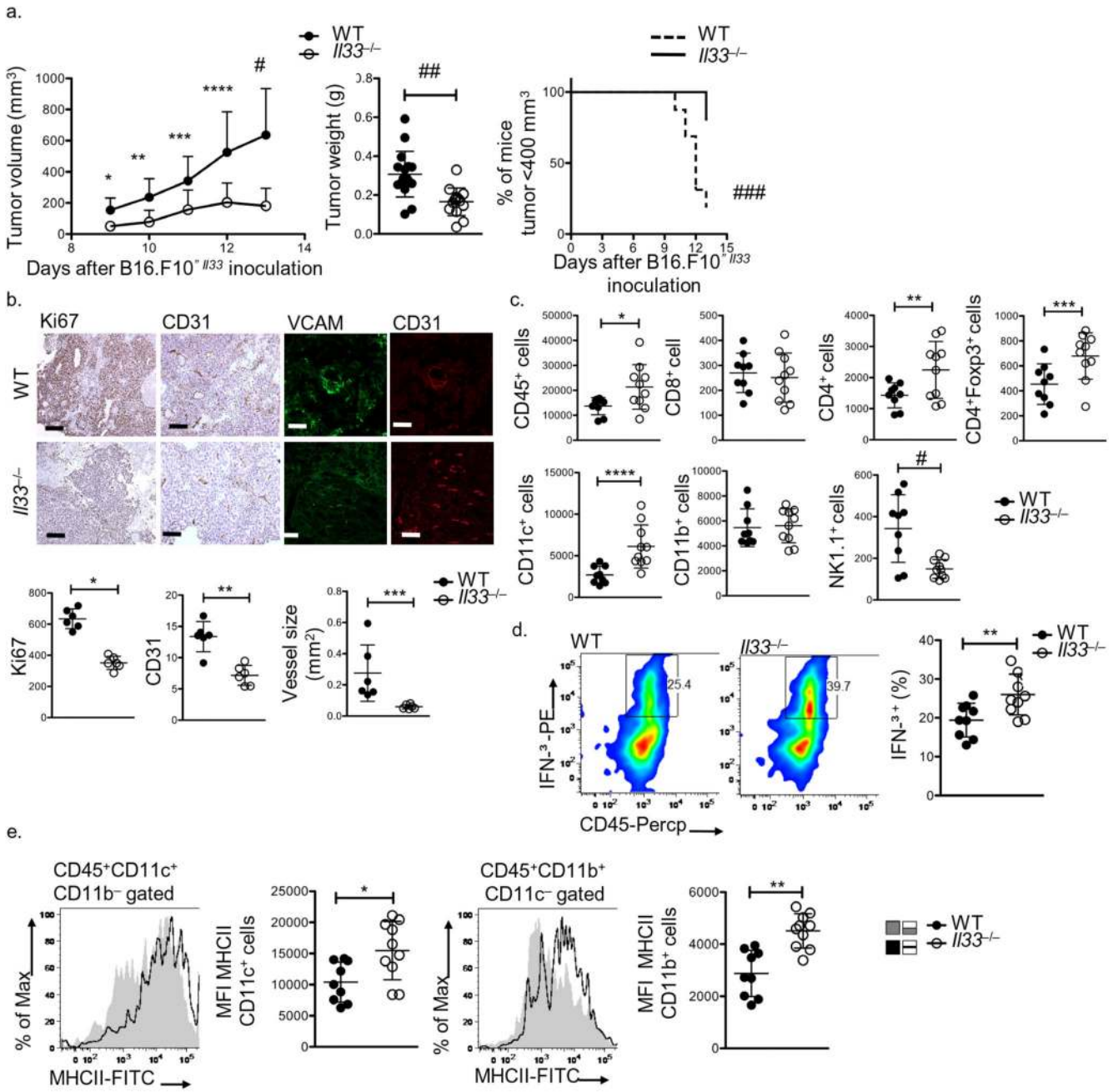

Figure 2. Host-derived IL-33 role in tumor regression.

(a) Tumor volume (mm^3) and % of mice bearing tumors <400 mm^3 of WT (n=9) and *Il33*$^{-/-}$ (n=10) mice 9-13 days following B16.F10$^{\Delta Il33}$ inoculation and tumor weight (g) on day 13. *P=0.0173, **P=0.0103, ***P=0.0158, ****P=0.0037, $^{\#}$P=0.0002, $^{\#\#}$P=0.0076, $^{\#\#\#}$P=0.0001 (b) Representative images of Ki67 and CD31 immunohistochemistry, VCAM and CD31 immunofluorescense and quantification plot of Ki67 intensity, CD31 intensity and vessel size from day 13 B16.F10$^{\Delta Il33}$ tumors from WT (n=6) and *Il33*$^{-/-}$ mice (n=6). 10 fields or more per tumor were quantified. Scale bars: Ki67=30 μm, CD31 immunohistochemistry=50 μm, CD31 and VCAM immunofluorescence=30 μm. *P<0.0001,

Europe PMC Funders Author Manuscripts

P=0.0004, ***P=0.0022 (c) Numbers per 5×10^5 tumor cells of $CD45^+$, $CD4^+$, $CD8^+$, $CD4^+Foxp3^+$, $CD11c^+$, $CD11b^+$, $NK1.1^+$ cells from day 13 $B16.F10^{\Delta Il33}$ tumors from WT (n=9) and $Il33^{-/-}$ (n=10) mice determined by FACS. *P=0.035, **P=0.0245, ***P=0.0123, ****P=0.0003, #P=0.0133, (d) Representative FACS plots and percentages of IFN-γ^+ cells derived from in vitro cultures of intratumoral $CD45^+$ cells of WT (n=9) and $Il33^{-/-}$(n=10) mice 13 days following $B16.F10^{\Delta Il33}$ inoculation. Numbers denote percentages of gated populations, **P=0.0088 (e) Representative overlays and MHCII MFI of $CD11c^+$ and $CD11b^+$ cells infiltrating $B16.F10^{\Delta Il33}$ day 13 tumors of WT (n=9) and $Il33^{-/-}$ mice (n=10). *P=0.0003, **P=0.0146. Data are shown as means ± SD. Representative data from five (a, c, d, e) independent experiments. (b, c**, c***, c****, d, e) unpaired two-tailed t-test, ($a^{\#\#}$, b***, c*, $c^{\#}$) Mann-Whitney two-tailed U-test, (a*, a**, a***, a****, $a^{\#}$) multiple unpaired two-tailed t-tests between WT and $Il33^{-/-}$ at each time point, ($a^{\#\#\#\#}$) two-tailed Log rank test. (a, b, c, d, e) n=biologically independent mouse samples.

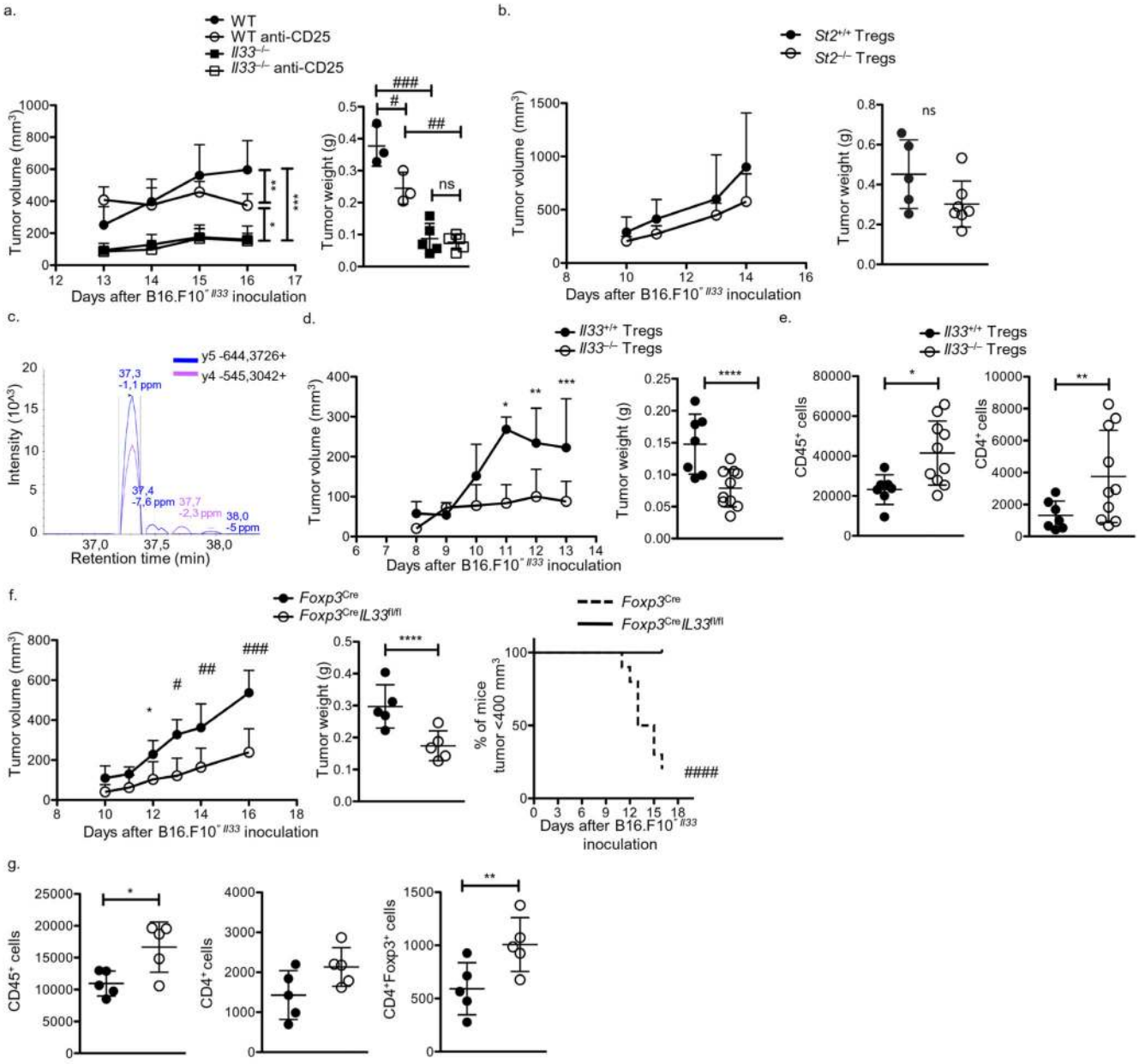

Figure 3. Impaired suppressive function of IL-33-deficient T_{reg} cells in vivo.

(a) Tumor volume (mm^3) and tumor weight (g) of B16.F10$^{\Delta Il33}$- inoculated control-injected or anti-CD25-depleted WT (n=3) and *Il33*$^{-/-}$ (n=5) mice. *P=0.016, **P=0.0005, ***P<0.001, #P=0.016, ##P=0.0012, ###P<0.0001, NS=0.975 (b) Tumor volume (mm^3) and tumor weight (g) (day 14) of B16.F10$^{\Delta Il33}$ inoculated *Rag1*$^{-/-}$ mice reconstituted with *St2*$^{+/+}$ T_{reg} cells (n=5) and *St2*$^{-/-}$ T_{reg} cells (n=7). NS=0.0996 (c) Intensity plot of the elution of y5 (m/z: 644.3726 charge: 1+) and y4 (m/z: 545.3042 charge: 1+) fragment ions of the IL-33 proteotypic peptide DYSVELQR (Aminoacids 198-205, m/z: 505.2511 charge:2+) extracted by protein extracts of in vitro activated lymph node WT CD4$^+$Foxp3$^+$ T_{reg} cells, separated by high performance liquid chromatography and injected in a Q Exactive mass spectrometer operating in Parallel Reaction Monitoring (PRM) mode (d)

Europe PMC Funders Author Manuscripts

Tumor volume (mm^3) and tumor weight (g) (day 13) of B16.F10$^{\Delta Il33}$ inoculated *Rag1*$^{-/-}$ mice reconstituted with *Il33*$^{+/+}$ T_{reg} cells (n=7) and *Il33*$^{-/-}$ T_{reg} cells (n=10). *P=0.0089, **P=0.0028, ***P=0.035, ****P=0.0021 (e) Numbers per 5×10^5 tumor cells of $CD45^+$ cells and $CD4^+$ T cells of *Il33*$^{+/+}$ T_{reg} cells (n=7) and *Il33*$^{-/-}$ T_{reg} cells-transferred (n=10) *Rag1*$^{-/-}$ mice. *P=0.0137, **P=0.0431 (f) Tumor volume (mm^3), tumor weight (g) and % of mice bearing tumors <400 mm^3 of B16.F10$^{\Delta Il33}$- inoculated *Foxp3*^{Cre} (n=5) and *Foxp3*^{Cre}*Il33*$^{fl/fl}$ (n=5) mice. *P=0.03, #P=0.0039, ##P=0.019, ###P=0.005, ****P=0.0101, ####P=0.0003. (g) Numbers per 5×10^5 tumor cells of $CD45^+$, $CD4^+$ and $CD4^+Foxp3^+$ T cells infiltrating day 16 tumors of B16.F10$^{\Delta Il33}$- inoculated *Foxp3*^{Cre} (n=5) and *Foxp3*^{Cre}*Il33*$^{fl/fl}$ (n=5) mice *P=0.031, **P=0.02. Data are shown as means ± SD. Representative data from two independent experiments. (b, d, e, g) unpaired two-tailed t-test, (b,d,f) multiple two-sided t-tests between WT and *Il33*$^{-/-}$ at each time point, (a) one-way two-tailed ANOVA with Tukey's multiple comparisons test, (f) two-tailed Log rank test. (a, b, d, e, f, g) n=biologically independent mouse samples.

Europe PMC Funders Author Manuscripts

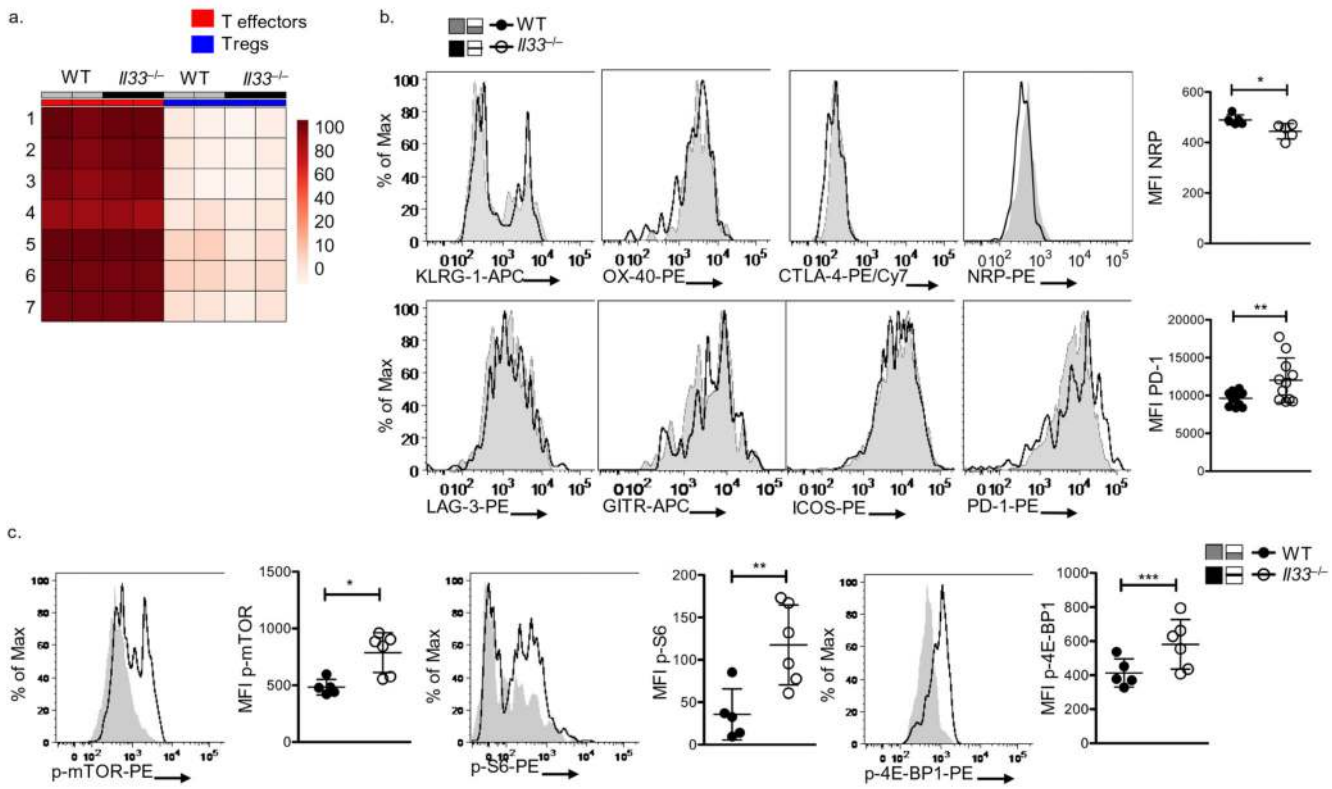

Figure 4. IL-33-deficient T_{reg} cells acquire a "fragile" phenotype.

(a) Color-coded methylation status (white=0% methylation, red=100% methylation) of individual CpG motifs (1-7) in the TSDR of *foxp3* gene in $CD4^+Foxp3^-$ (Teffectors) and $CD4^+Foxp3^+$ cells (T_{reg} cells) infiltrating tumors of WT (n=4) and *Il33*$^{-/-}$ (n=4) mice (b) Histogram overlays of KLRG-1, OX-40, CTLA-4, LAG-3, GITR, ICOS, NRP and PD-1 expression and plots of PD-1 (n=11) and NRP (n=5) MFI of tumor-infiltrating T_{reg} cells ($CD4^+Foxp3^+$) from WT and *Il33*$^{-/-}$ mice. *P=0.023, **P=0.0133 (c) Overlays and MFI of pmTOR, pS6, p4E-BP1 from intratumoral T_{reg} cells ($CD4^+Foxp3^+$) of WT (n=5) and *Il33*$^{-/-}$ (n=6) mice. *P=0.0056, **P=0.0085, ***P=0.0487. Data are shown as means ± SD. Representative data from two independent experiments. unpaired two-tailed t-test. (a, b, c) n=biologically independent mouse samples.

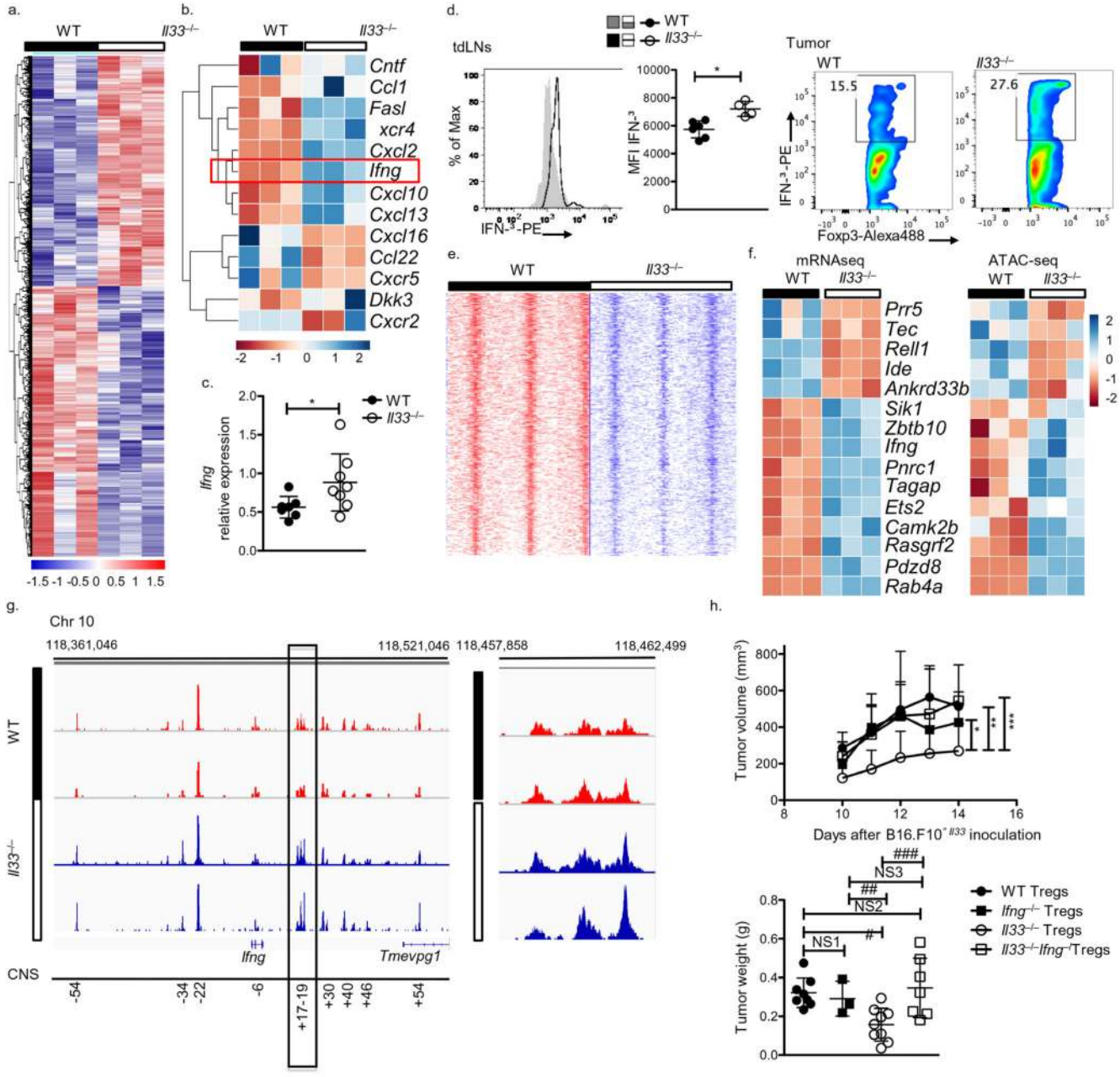

Figure 5. Role of IFN-γ in the impaired suppressive function of *Il33*$^{-/-}$ T_{reg} cells.

(a) Heatmap of differentially expressed genes of tdLNs T_{reg} cells ($CD4^+CD25^+GITR^+Foxp3^+$) from WT (n=3) and *Il33*$^{-/-}$ (n=3) mice. (b) Heatmap of differentially expressed cytokines, chemokines and chemokine receptors genes of tdLNs T_{reg} cells from WT (n=3) and *Il33*$^{-/-}$ (n=3) mice (c) Relative expression of IFN-γ in tdLNs T_{reg} cells from WT (n=7) and *Il33*$^{-/-}$ (n=8), *P=0.0401 (Mann-Whitney two-tailed U-test) (d) Representative overlay and MFI of IFN-γ produced by T_{reg} cells from tdLNs of WT (n=6) and *Il33*$^{-/-}$ (n=4) mice and percentages of IFN-γ positive T_{reg} cells from $CD45^+$ tumor infiltrating cells following in vitro activation *P=0.0469 (unpaired two-tailed t-test) (e) Heatmaps demonstrating normalized ATAC-seq tag counts around 1595 loci (+/- 1.25 kb window) of tdLNs T_{reg} cells

Europe PMC Funders Author Manuscripts

from WT (n=3) and *Il33*$^{-/-}$ (n=3) mice (f) Heatmaps of genes exhibiting simultaneous differential chromatin accessibility and gene expression of tdLNs T_{reg} cells from WT (n=3) and *Il33*$^{-/-}$ (n=3) mice (g) ATACseq signal profiles across *Ifng* locus (Chromosome 10: 118.361.046-118.521.046 bp) and *Ifng* CNS +17/+19 (Chromosome 10: 118.457.858-118.462.499) of tdLNs T_{reg} cells from WT (n=6) and *Il33*$^{-/-}$ mice (n=4) (h) Tumor volume (mm^3) and tumor weight (g) (day 14) of B16.F10$^{\Delta Il33}$ inoculated *Rag1*$^{-/-}$ mice adoptively transferred with T_{reg} cells from WT (n=8), *Ifng*$^{-/-}$ (n=3), *Il33*$^{-/-}$ (n=9) and *Il33*$^{-/-}$*Ifng*$^{-/-}$ mice (n=7). *P=0.049, **P<0.0001, ***P=0.0279, #P=0.019, ##P=0.0129, ###P=0.0085, NS1=0.9745, NS2=0.9678, NS3=0.8742 (one-way ANOVA with Tukey's multiple comparisons test). Data are shown as means ± SD. (a, b, f) Color corresponds to per gene z-score normalized FPKM counts across samples and genes are hierarchically clustered. (a, b, c, d, e, f, g, h) n=biologically independent mouse samples.

Europe PMC Funders Author Manuscripts

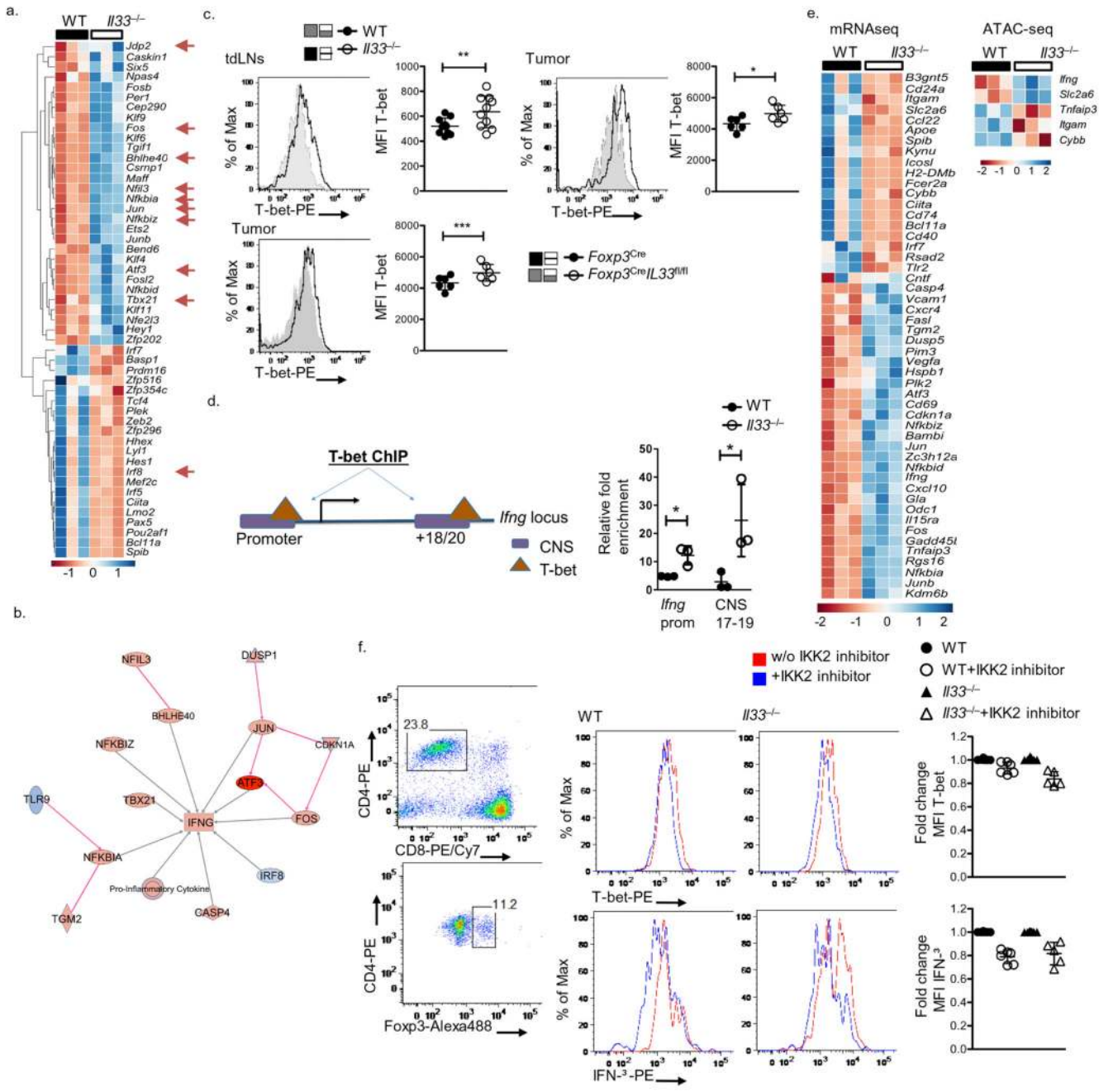

Figure 6. Increased NF-κB activation and T-bet expression promote IFN-γ production in *Il33*$^{-/-}$ Foxp3^{+} T$_{reg}$ cells.

(a) Heatmap of the differentially expressed transcription regulators of tdLNs T$_{reg}$ cells (CD4^{+}CD25^{+}GITR^{+}Foxp3^{+}) from WT (n=3) and Il33$^{-/-}$ (n=3) mice. Arrows indicate transcription regulators of IFN-γ (b) Ingenuity Pathway Analysis of IFN-γ upstream regulators. The molecules color represents the expression levels (log2): blue=underexpressed, red=overexpressed in *Il33*$^{-/-}$ samples compared to WT samples (c) Representative overlays and MFI of T-bet expression in tumor-infiltrating T$_{reg}$ cells (WT n=6, *Il33*$^{-/-}$ n=6, *Foxp3*^{Cre}=3, *Foxp3*^{Cre}IL33$^{fl/fl}$=3) and tdLNs T$_{reg}$ cells (WT n=10, *Il33*$^{-/-}$

Europe PMC Funders Author Manuscripts

n=10) of B16.F10$^{\Delta Il33}$ inoculated mice. *P=0.0454, **P=0.0201, ***P=0.019 (unpaired two-tailed t-test). Data are shown as means ± SD (d) Relative fold enrichment of T-bet binding (anti T-bet/IgG) to IFN-γ promoter and CNS17-19 by ChIP performed on chromatin derived from tdLNs T_{reg} cells. Results from 2 independent experiments from pooled WT (n=4) and *Il33*$^{-/-}$ (n=4) mice *p=0.0178, unpaired Student two-tailed t test. Data are shown as means ± SD (e) Heat map of differentially expressed and differentially accessible NF-κB target genes of tdLNs T_{reg} cells from WT (n=3) and *Il33*$^{-/-}$ (n=3) mice (f) Representative overlays of T-bet and IFN-γ expression and gating strategy of WT (n=6) and *Il33*$^{-/-}$ (n=5) CD4^{+}CD8^{-}Foxp3^{+} T_{reg} cells in two days tdLN cell culture with aCD3/aCD28 beads in the presence or absence of IKK2 inhibitor. MFI of T-bet and IFN-γ is normalized to the MFI of T_{reg} cells cultured in the absence of IKK2 inhibitor. Data are shown as means ± SD (c, d) Representative data of three independent experiments. (a, e) Color corresponds to per gene z-score normalized FPKM counts across samples and genes are hierarchically clustered. (a, c, d, e, f) n=biologically independent mouse samples.

Europe PMC Funders Author Manuscripts

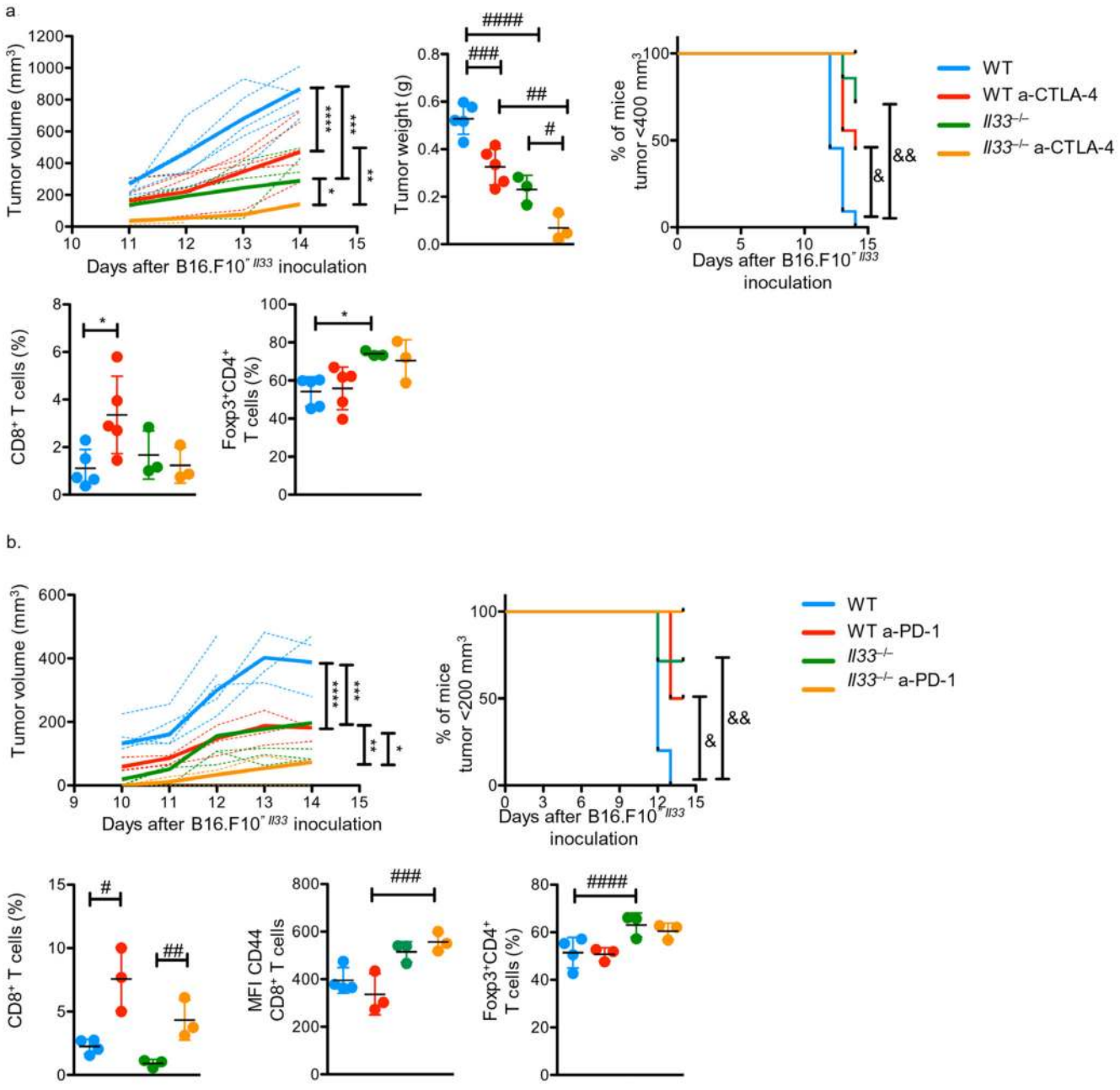

Figure 7. IL-33 deficiency potentiated immunotherapy efficacy.

(a) Tumor volume (mm^3) curve (days 11-14), % of mice bearing tumors <200 or 400 mm^3 and tumor weight (g), percentages and CD44 MFI of $CD8^+$ and percentages of $Foxp3^+CD4^+$ T cells in TILs ($CD45^+$) (day 14) of B16.F10$^{\Delta Il33}$ inoculated control and aCTLA-4 (b) or aPD-1 (c) treated WT (n=5, 4) and *Il33*$^{-/-}$ (n=3) mice. Data are shown as means ± SD a*P=0.0421, a**P=0.0048, a***P=0.0081, a****P=0.0161, a#P=0.0517, a##P=0.0010, a###P=0.0022, a####P=0.0003, b*P=0.0484, b**P=0.0033, b***P=0.0069, b****P=0.0017, b#P=0.0159, b##P=0.0159, b###P=0.016, b####P=0.04 (one-way ANOVA with Tukey's multiple comparisons test), a&P=0.0022, a&&P=0.0004, b&P=0.0187,

Europe PMC Funders Author Manuscripts

b&&P=0.0158 (Log rank test). Representative data from two independent experiments. (a, b, c) n=biologically independent mouse samples.

Europe PMC Funders Author Manuscripts